Title

Colonization Dynamics Explain the Decoupling of Species Richness and Morphological Disparity in Syngnatharian Fishes across Oceans.

Journal

The American Naturalist, 205(3)

ISSN

0003-0147

Authors

Santaquiteria, Aintzane

Miller, Elizabeth Christina

Rosas-Puchuri, Ulises

et al.

Publication Date

2025-03-01

DOI

10.1086/733931

E-Article

Colonization Dynamics Explain the Decoupling of Species Richness and Morphological Disparity in Syngnatharian Fishes across Oceans

Aintzane Santaquiteria,[1,2,*] Elizabeth Christina Miller,[1] Ulises Rosas-Puchuri,[1] Carmen del R. Pedraza-Marrón,[1,3] Emily M. Troyer,[1] Mark W. Westneat,[4] Giorgio Carnevale,[5] Dahiana Arcila,[6] and Ricardo Betancur-R.[6,*]

1. School of Biological Sciences, University of Oklahoma, Norman, Oklahoma 73019; 2. Department of Biological Sciences, George Washington University, Washington, DC 20052; 3. Department of Life and Environmental Sciences, University of California, Merced, California 95343; 4. Department of Organismal Biology and Anatomy, University of Chicago, Chicago, Illinois 60637; 5. Dipartimento di Scienze della Terra, Università degli Studi di Torino, Torino 10125, Italy; 6. Marine Biology Research Division, Scripps Institution of Oceanography, University of California, San Diego, California 95037

Submitted February 7, 2024; Accepted October 21, 2024; Electronically published January 17, 2025

Online enhancements: supplemental PDF.

ABSTRACT: A clear longitudinal gradient in species richness across oceans is observed in extant marine fishes, with the Indo-Pacific exhibiting the greatest diversity. Three non-mutually-exclusive evolutionary hypotheses have been proposed to explain this diversity gradient: time for speciation, center of accumulation, and in situ diversification rates. Using the morphologically disparate syngnatharians (seahorses, dragonets, goatfishes, and relatives) as a study system, we tested these hypotheses and additionally assessed whether patterns of morphological diversity are congruent with species richness patterns. We used well-sampled phylogenies and a suite of phylogenetic comparative methods (including a novel phylogenetically corrected Kruskal-Wallis test) that account for various sources of uncertainty to estimate rates of lineage diversification and morphological disparity within all three major oceanic realms (Indo-Pacific, Atlantic, and eastern Pacific), as well as within the Indo-Pacific region. We find similar lineage diversification rates across regions, indicating that increased syngnatharian diversity in the Indo-Pacific is due to earlier colonizations from the Tethys Sea followed by in situ speciation and more frequent colonizations during the Miocene coinciding with the formation of coral reefs. These results support both time for speciation and center of accumulation hypotheses. Unlike species richness unevenness, shape disparity and evolutionary rates are similar across oceans because of the early origin of major body plans and their subsequent spread via colonization rather than in situ evolution. Our results illustrate how species richness patterns became decoupled from morphological disparity patterns during the formation of a major biodiversity hot spot.

Keywords: diversity gradients, historical biogeography, ultraconserved elements (UCEs), dispersal, morphology.

* Corresponding authors; email: aintzanesantaquiteria@gmail.com, rbetancur@ucsd.edu.

ORCIDs: Santaquiteria, https://orcid.org/0000-0002-7046-6434; Miller, https://orcid.org/0000-0001-6856-3107; Rosas-Puchuri, https://orcid.org/0000-0003-0529-2623; Pedraza-Marrón, https://orcid.org/0000-0002-2692-4610; Troyer, https://orcid.org/0000-0001-7478-2306; Westneat, https://orcid.org/0000-0002-3548-7002; Carnevale, https://orcid.org/0000-0002-3433-4127; Arcila, https://orcid.org/0000-0002-5126-1345; Betancur-R., https://orcid.org/0000-0002-9512-5011.

Introduction

Three processes directly change the species richness of a region: speciation, extinction, and dispersal (Ricklefs 1987). Variation in the rates and timing of these processes are responsible for shaping diversity gradients such as those observed along latitudinal (Rolland et al. 2014), longitudinal (Cowling et al. 2017), elevation (Vasconcelos et al. 2020), and depth (Miller et al. 2022) gradients. The mechanisms behind this variation are ultimately a combination of biotic and abiotic factors, such as climatic stability, geographical barriers, productivity, competition, and predation (Mittelbach et al. 2007; Edgar et al. 2017).

Multiple non-mutually-exclusive hypotheses have been proposed to explain species richness patterns from an evolutionary process perspective (e.g., Gaboriau et al. 2019). The time for speciation hypothesis (Stephens and Wiens 2003), sometimes referred to as the museum hypothesis, suggests that earlier colonization of regions provides lineages

  https://doi.org/10.1086/733931

with more time to diversify, ultimately leading to higher species richness. The center of accumulation hypothesis (Ladd 1960) posits that higher diversity of a region is due to preferential colonization. A highly diverse region may subsequently act as a source, with species dispersing to new regions, or as a sink where colonization outpaces outward dispersal (Jablonski et al. 2006). The center of origin or in situ diversification rate hypothesis (Briggs 1974; Rohde 1992), sometimes referred to as the cradle, posits that regions with higher rates of speciation will exhibit greater species richness. Other hypotheses that remain largely untested include the center of survival, which suggests that the stability of an area may enable persistence, leading to increased species diversity (Barber and Bellwood 2005), and the center of overlap hypothesis, which posits that species with widespread ranges tend to overlap more in centrally positioned areas, leading to increased diversity in those areas (Woodland 1983). Recent macroevolutionary studies focusing on diversity gradients have emphasized time for speciation as a prominent explanatory factor in various clades, including freshwater (Miller and Román-Palacios 2021; García-Andrade et al. 2023) and marine (Miller et al. 2018) fishes, terrestrial turtles (Stephens and Wiens 2003), and plants (Cowling et al. 2017). Some studies have also observed lower diversification rates in regions with high species richness, as seen for marine fishes along a latitudinal diversity gradient (Rabosky et al. 2018), although the reverse is true for amphibians, mammals, and certain groups of reef fishes that have higher speciation rates in the tropics (Pyron and Wiens 2013; Rolland et al. 2014; Siqueira et al. 2016).

Despite extensive research into the factors contributing to the heterogeneity of species richness across regions, studies assessing the temporal relationship between species richness and morphological or functional diversity have received far less attention (Crouch and Jablonski 2023; Diamond and Roy 2023). Here, we consider three potential relationships between morphological and lineage diversity: no correlation, a positive correlation, or a negative correlation. Disparity and richness can be decoupled if regions with varying levels of species richness exhibit similar levels of morphological disparity and rates of trait evolution. This can happen if regions have similar environmental and ecological pressures that generate functional redundancy, including via morphological convergence, where distantly related species can perform similar functional roles leading to morphological overlap across regions (Ricklefs 2012; Mouillot et al. 2014; Price et al. 2015; McLean et al. 2021). Uncorrelated patterns may also arise because all major body plans in a group originated before the group dispersed to other regions (Friedman 2010). On the other hand, species-poor areas (e.g., temperate zones) may exhibit greater morphological disparity because of in situ evolution. This could happen because of the increased ecological opportunity resulting from lower biotic interactions, compared with regions with higher species richness where competition may be elevated, thereby promoting faster rates of morphological evolution (Lawson and Weir 2014; Burns et al. 2024). This second scenario would result in an inverse relationship between morphological disparity and species richness (Hipsley et al. 2014; López-Martínez et al. 2024). Finally, richness and disparity can be positively correlated, especially within biodiversity hot spots. This can be attributed to the emergence of novel niches (Schluter 2015), such as specialized diets (Kissling et al. 2012), thereby promoting trait evolution. Alternatively, it may result from these regions being colonized earlier, allowing more time for morphological evolution (similar to the time for speciation hypothesis), in which case morphological evolutionary rates do not vary across the gradient.

Most studies on species richness and morphological diversity focus on the latitudinal diversity gradient in terrestrial organisms (e.g., Drury et al. 2021), with some also examining marine fishes (e.g., Burns et al. 2024). Less attention has been given to longitudinal patterns. For example, shallow marine groups show a clear longitudinal gradient in species richness across the oceans, with higher diversity observed in the Indo-Pacific (IP) compared with the eastern Pacific (EP) and Atlantic (Atl) oceans (e.g., Tittensor et al. 2010; Edgar et al. 2017). Species richness peaks within the central Indo-Pacific (CIP), a subregion of the IP that includes the Indo-Australian archipelago (IAA) diversity hot spot (Renema et al. 2008). The hypotheses given above have been individually proposed to explain the processes driving the high biodiversity of the CIP, although it is now believed that present-day reef fish distributions are the result of a combination of accumulation, survival, in situ speciation (e.g., Bowen et al. 2013; Bellwood et al. 2015), and earlier colonization (Miller et al. 2018).

Researchers have also examined morphological diversity in reef fishes from a biogeographic perspective, investigating various ecological and morphological traits like diet, habitat, body size, and body shape (Mouillot et al. 2014; Siqueira et al. 2019; McLean et al. 2021; Diamond and Roy 2023; Burns et al. 2024). To date, global-scale studies including all reef-associated fishes have identified trait similarities between marine realms, suggesting shared functional roles across biogeographic communities (Mouillot et al. 2014; McLean et al. 2021). However, within individual reef-associated clades (e.g., surgeonfishes, rabbitfishes, and parrotfishes), greater disparity has been observed in the IP compared with the Atl (Siqueira et al. 2019), possibly because of the highly complex and structurally diverse coral formations providing more available niches in the former (Sanciangco et al. 2013). This example illustrates how the different phylogenetic scales across studies can lead to different findings,

with both types of studies providing value. Studies focused on a single clade can offer insights into specific biological processes that are often obscured in global-scale analyses because of the lack of detail (Clarke 2021). By focusing on a single clade that follows the same global pattern of interest, it is possible to meticulously trace its evolutionary history and ecological dynamics, thereby achieving a more precise understanding of the underlying patterns and processes.

The teleost clade Syngnatharia (669 species), which includes seahorses, pipefishes, flying gurnards, goatfishes, dragonets, and sea moths, offers an excellent opportunity to investigate the extent to which species richness and morphological patterns found on a global scale (Miller et al. 2018; McLean et al. 2021) are also reflected within a single marine clade. This diverse clade is widely distributed across the globe and exhibits the same longitudinal diversity gradient seen across all marine fishes (Miller et al. 2018). Originating in the ancient Tethys Sea during the Late Cretaceous (Santaquiteria et al. 2021; Stiller et al. 2022), syngnatharian lineages have since colonized tropical and temperate biogeographic regions across the globe and diversified in various habitats, including seagrass beds, coral and rocky reefs, and mangrove forests (Froese and Pauly 2021; Santaquiteria et al. 2021; Stiller et al. 2022). The IP region has the highest syngnatharian species richness (~535 species), far surpassing other oceanic realms (Atl: ~94 species; EP: ~29 species). Additionally, compared with other fish clades of similar age, syngnatharians are exceptional in exhibiting a great diversity of body plans and novelties, including elongated snouts and bodies, prehensile tails, and hyoid barbels (Neutens et al. 2014; Nash et al. 2022), rendering them an ideal system for assessing morphological disparity with geography.

Here, we examine lineage diversification and body shape morphometrics broadly across Syngnatharia, considering their associations with different biogeographic regions. We aim to understand the evolutionary processes influencing the longitudinal diversity gradient from a diversity and disparity perspective. Specifically, we ask whether the higher species richness in the IP is explained by the time for speciation, center of accumulation (more colonization events), and/or center of origin (higher in situ diversification rates) hypotheses. Additionally, we investigate the morphological disparity along the longitudinal axis to assess the degree of correlation with the species richness gradient. To test these hypotheses, we first expanded on prior phylogenomic analyses of Syngnatharia (Santaquiteria et al. 2021) to include a total of 323 species (~50% of the species diversity). We then conducted a suite of comprehensive phylogenetic comparative methods that carefully consider uncertainties in topology, divergence times, and other sources of variation.

Methods

See the supplemental PDF for additional methodological details.

Taxonomic Sampling, Phylogenetic Inference, and Tree Uncertainty

The phylogenetic framework for our comparative analyses builds on two previous studies that examined the evolutionary and biogeographic history of syngnatharians based on ultraconserved elements (UCEs; 932 loci) sequenced from 163 species (Longo et al. 2017; Santaquiteria et al. 2021). To account for tree uncertainty in downstream comparative analyses (see Santaquiteria et al. 2021), we estimated 56 backbone time trees, 28 dated with MCMCTree (dos Reis and Yang 2019) and 28 dated with RelTime (Tamura et al. 2012), using as input topologies from alternative UCE matrices analyzed with both maximum likelihood (14 RAxML trees; Stamatakis 2014) and coalescent (14 ASTRAL-III trees; Mirarab and Warnow 2015) approaches. To improve taxonomic representation in our analyses, we expanded the sampling on all backbone trees by incorporating 160 additional syngnatharian taxa via publicly available mitochondrial sequences. This expansion covered approximately 50% of the extant diversity within the group, accounting for 323 of 669 species (see app. 1, available in the Dryad Digital Repository [https://doi.org/10.5061/dryad.zkh1893gd; Santaquiteria et al. 2024]). We rigorously vetted these sequences through a series of quality control steps and considered discrepancies in phylogenetic placement compared with a recent phylogenomic study (Stiller et al. 2022). For time calibration, we used a combination of 13 primary calibrations, including four new calibrations, placed on the backbone trees. After backbone trees were calibrated using MCMCTree and RelTime, multiple secondary calibrations were then placed on the expanded trees using congruification (Eastman et al. 2013) in conjunction with treePL (Smith and O'Meara 2012).

Biogeographic History and Timing of Regional Colonization

We estimated ancestral ranges using the R package BioGeoBEARS (Matzke 2013) following the approach outlined in Santaquiteria et al. (2021) to incorporate phylogenetic uncertainty. We built a presence/absence matrix by coding each extant species according to its geographic range based on a seven-area biogeographic scheme (Spalding et al. 2007; Kulbicki et al. 2013): western Indian Ocean (WIO), CIP, central Pacific (CP), temperate Australasia (TA), tropical eastern Pacific (TEP), western Atlantic (WA), and eastern

Atlantic (EA). We also used paleogeographic domain information as biogeographic constraints based on data obtained from the 10 fossils used to calibrate our trees, adding the ancient Tethys Sea as the eighth area. We evaluated 12 biogeographic models (table S5; tables S1–S7 are available online) using three time slices (92–12, 12–2.8, and 2.8–0 Ma) and a connectivity matrix based on dispersal probabilities between regions that change with continental rearrangements. As the summary phylogeny, we used the "master" tree (expanded RAxML tree inferred using the 932-UCE backbone tree and dated in RelTime). On the basis of the sensitivity of biogeographic inferences previously identified for the group, we accounted for both topological uncertainty and inclusion/exclusion of the jump dispersal or founder speciation event (*j* parameter), which favors long-distance dispersal events, in biogeographic models (Ree and Sanmartín 2018; Matzke 2022). We summarized ancestral range estimates from all 28 RelTime trees by overlying average probabilities across compatible nodes on the master tree (Matzke 2019) using the best-fit model with (+*j*) and without (−*j*) the *j* parameter.

We assessed the center of accumulation and time for speciation hypotheses by estimating the frequency and timing of colonization events between areas. To accomplish this, we conducted biogeographic stochastic mapping analyses by simulating 100 stochastic histories on the master tree based on the best-fit biogeographic models (Dupin et al. 2017). From each stochastic map, we extracted the ranges at every node and tip, identifying all individual colonizations, their descendants, and the timing of colonization for each region. For each region, we then calculated the number of cumulative lineages (because of a combination of colonization and speciation), number of independent colonization events, immigration and emigration rates, speciation rates, and extirpation rates across time by averaging across 100 histories. This approach follows the biogeographic methodology developed by Xing and Ree (2017) and implemented previously (e.g., Ding et al. 2020; Miller et al. 2022). We repeated all biogeographic analyses using the "alternative" tree (expanded RAxML tree inferred using the 932-UCE backbone tree and dated in MCMCTree) and all 28 MCMCTree trees.

Diversification Rates among Regions

To assess the influence of geographic distribution on lineage diversification dynamics (testing the in situ diversification rates hypothesis), we estimated diversification rates based on the set of 56 expanded phylogenies and three different approaches for calculating rates. We also assessed the sensitivity of diversification rate analyses to 12 terminal nodes with shallow divergences (i.e., T-like terminal nodes with branch lengths <0.5 Ma), which may indicate taxonomic oversplitting and can "force" models to fit extremely fast rates. For geographic-dependent analyses, we fitted 24 different area-independent and area-dependent models in GeoHiSSE (Caetano et al. 2018), both with and without the *j* parameter (table S4). Because GeoHiSSE allows comparisons of only two regions at a time, we analyzed each focal area against the remaining areas: IP vs. EP + Atl, EP vs. IP + Atl, and Atl vs. IP + EP. From these comparisons, we extracted only the tip-associated diversification rates for each focal area (IP, Atl, and EP), without performing statistical pairwise tests. We calculated the sampling fractions for each region across all comparisons (IP: 47.85%; EP: 65.52%; Atl: 65.96%). We then estimated the Akaike information criterion (AIC) values for each of the models and averaged tip-associated rates from the best three models (~95% accumulative weight) using Akaike weights. To estimate diversification rates in Bayesian Analysis of Macroevolutionary Mixtures (BAMM ver. 2.5.0), for each tree, we estimated prior parameters for time-variable speciation and extinction models using the R package BAMMTools (Rabosky et al. 2014). After running BAMM independently for each tree, we combined all results by calculating the mean diversification rate for each tip. Finally, we also estimated tip rates using the DR statistics function for each tree (Jetz et al. 2012).

For each analysis, we compared mean tip-associated lineage diversification rates between (i) all oceanic realms (IP, EP, and Atl), (ii) all subareas within the IP (WIO, CIP, CP, and TA), and (iii) both sides of the Atl (EA and WA). We conducted these analyses for all syngnatharian lineages, as well as within four separate suborder-level clades in isolation—Syngnathoidei, Callionymoidei, Mulloidei, and Dactylopteroidei—to account for phylogenetic scale (Clarke 2021; Miller et al. 2021; fig. 1). Residual errors from lineage diversification rates were not normally distributed (even after log transformation). Therefore, to assess statistical significance of tip-rate differences among the different biogeographic regions, we implemented a novel phylogenetically corrected nonparametric Kruskal-Wallis test (see the supplemental PDF for more details). Briefly, we placed the values of diversification rates into a vector and then multiplied this vector by the inverse of the square root of the covariance matrix (i.e., if this matrix is denoted as $\mathbf{P}$, then $\mathbf{P} = \mathbf{Q}\Lambda^{-1/2}\mathbf{Q}^{\top}$, where $\mathbf{Q}$ and $\mathbf{\Lambda}$ are the matrices of eigenvectors and eigenvalues of the covariance matrix, respectively; Garland and Ives 2000). By doing so, the diversification rates were weighted in this manner by the phylogeny, and we applied the Kruskal-Wallis test to these values. If the *P* values were significant, we ran a pairwise comparison using the kwAllPairsConoverTest function with Bonferroni correction implemented in the R package PMCMRplus (Pohlert 2021). For each statistical test

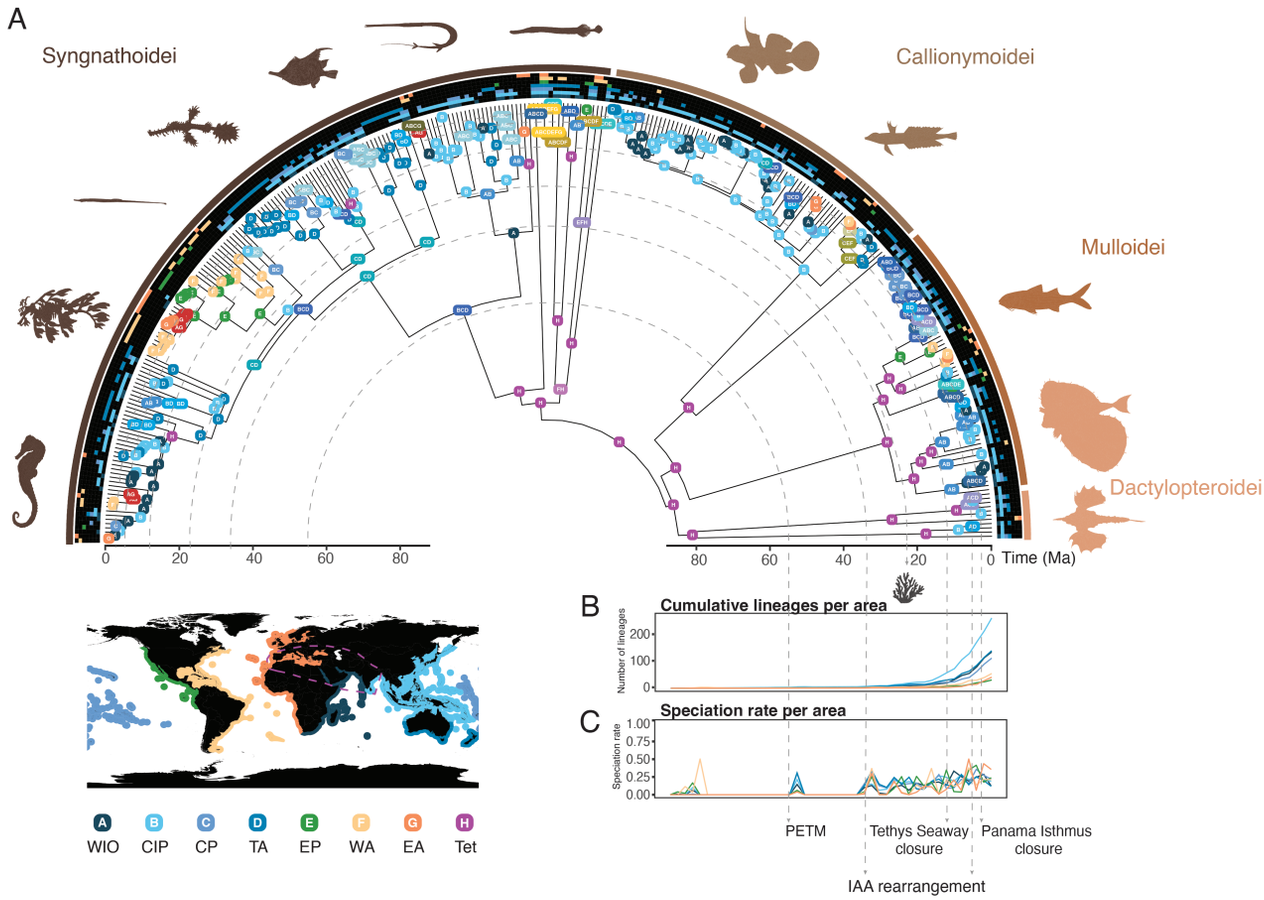

Figure 1: Syngnatharian phylogeny (323 species based on 932 ultraconserved elements and the cytochrome oxidase subunit I or COI marker) biogeographic history (*A*) and regional lineage accumulation (*B*) and speciation rates (*C*) over time based on ancestral range inferences and biogeographic stochastic mapping. The central Indo-Pacific (CIP) has accrued the largest number of lineages, experiencing a steep increase after the closure of the Tethys Seaway. Speciation rates are synchronous across areas, with three notable increases. Boxes at nodes are color-coded by area or areas with the highest maximum likelihood probability; the heat map in front of the tips represents the distribution of extant species. Major geological events are depicted with dotted lines: Paleocene-Eocene Thermal Maximum (PETM; ~56 Ma), Indo-Australian archipelago (IAA; 33.9–5.3 Ma) rearrangement (associated with the expansion of modern coral reef formations), Tethys Seaway closure (12 Ma), and the closure of the Isthmus of Panama (2.8 Ma). WIO = western Indian Ocean; CP = central Pacific; TA = temperate Australasia; EP = eastern Pacific; WA = western Atlantic; EA = eastern Atlantic; Tet = Tethys Sea. For complementary analyses, see figures S5–S9 and S13–S16.

conducted across the different methods, we set the degree of confidence to 95% and estimated the degrees of freedom, χ^2 values, and *P* values. For visualization purposes, the data are presented as nontransformed in "Results" and as log transformed in the figures.

Morphological Disparity and Rates by Region

To assess phenotypic disparity across biogeographic regions, we used two-dimensional geometric morphometric analyses to examine morphospace occupation and evolutionary rates within major oceanic realms as well as within subareas of the IP. We performed all morphological analyses considering all syngnatharian species and also within each suborder, as the results obtained with the entire clade may be obscured by the outstanding morphological disparity across the group. We placed a total of 12 landmarks and two semilandmarks using lateral photographs from 474 specimens in 171 species (two to five specimens to account for intraspecific variation) sourced from museum collections (e.g., Smithsonian) and other online repositories (Bray and Gomon 2021; Froese and Pauly 2021). To accommodate seahorse, pigmy pipehorse, and sea dragon specimens with bent body structures, we created two alternative

schemes: a head-only set (including these specimens) and a full-body set (excluding them; fig. S1; figs. S1–S38 are available online). We used the R package geomorph (Adams et al. 2021) to summarize variation in syngnatharian morphology using Procrustes superimposition, which corrects for size, scale, and rotation while calculating species-average coordinates. Using all 56 trees as input, we then conducted a principal component analysis (PCA) as well as a phylogenetically corrected PCA (pPCA) using phytools (Revell 2012). For downstream morphological analyses, we selected PCs and pPCs explaining 95% of the variation (one to four axes for the head-only shape and one to six axes for the full-body shape; see "Results").

To quantify the morphospace occupancy of syngnatharians in each of the major biogeographic regions, we calculated the overlap (Jaccard and Sørenson statistics) between each region using the R package hypervolume (Blonder et al. 2018). We used pPC scores obtained from the master tree and the alternative tree as input. We created four-dimensional hypervolumes for the head-only scheme and six-dimensional hypervolumes for the full-body scheme. To examine contemporary trait disparity in syngnatharians, we used the R package dispRity (Guillerme 2018). Using the dispRity.per.group function, we calculated the sum of variances for each biogeographical region based on both landmark schemes using PC and pPC scores as input. We also analyzed disparity through time in syngnatharians using pPC scores obtained from our master tree and alternative tree, by calculating the sum of variance metric using the dtt.dispRity function in dispRity. We then evaluated the fit of eight morphological evolutionary models in the R package mvMORPH (Clavel et al. 2015) using pPC and PC scores for each scheme across all trees (RelTime and MCMCTree): (i) a single-rate Brownian motion (BM), (ii) a single-regime Orstein-Uhlenbeck (OU), (iii) an early burst (EB), (iv) multiregime BM, (v) multiregime OU, (vi) EB to independent rates OU shift, (vii) BM to independent rates OU shift, and (viii) EB to independent rates BM shift. For the models with multiple regimes and shifts, we applied a trait change at 78 Ma across the tree, as we observed a steep decline of the morphological disparity at this time that also coincides with the origination of suborders (see "Results"). Finally, to assess morphological evolutionary rates within areas, we estimated rates for each syngnatharian lineage across regions in BAMM, with the caveat that each PC/pPC needed to be analyzed separately (Uyeda et al. 2015). We ran BAMM independently for all 56 trees. We then combined the MCMC results from all selected PCs and pPCs and calculated mean rates for each lineage across the 28 RelTime trees and the 28 MCMCTree trees. Last, we compared the statistical significance of morphological rates between realms and IP regions using the modified Kruskal-Wallis test as explained for diversification rates (see above).

Results

See the supplemental PDF for extended results.

Biogeographic History and Timing of Regional Colonization

The best-supported biogeographic model in our ancestral range reconstruction analyses was BAYAREA+*j* (table S5). Considering recent criticisms on the implementation of the jump dispersal parameter (*j*), we conducted the biogeographic analyses and interpreted the results herein with and without this parameter. Ancestral range reconstructions are similar to those obtained in previous studies for Syngnatharia (fig. 1*A*; Santaquiteria et al. 2021; Stiller et al. 2022; see also fig. S37). Ancestral syngnatharian lineages originated in the Tethys Sea in the Late Cretaceous around 87 Ma. Syngnathids (seahorses and pipefishes) subsequently dispersed eastward into the IP around 52 Ma, right after the Paleocene-Eocene Thermal Maximum (PETM). The remaining families dispersed into the IP more recently, during the Miocene and the IAA rearrangement (20 Ma on). Finally, all major families except pegasids (sea moths) colonized the Atl and the EP multiple times via alternative routes (figs. 1*A*, S6; see also Santaquiteria et al. 2021). The BAYAREA results without the *j* parameter show similar patterns but with more widespread ancestral distributions (fig. S7). Finally, results obtained using MCMCTree trees are similar, except that ancestral colonizations are inferred to have occurred ~10 million years earlier (figs. S8, S9).

On the basis of analyses of biogeographic stochastic histories, we find that more than 50% of syngnatharian lineages have similar dispersal rates from the Tethys Sea into the WIO, CIP, and WA regions (0.037–0.045), with the highest dispersal rate observed into CIP (0.045; fig. 2*A*). Lineages began colonizing the IP more frequently around 23 million years ago, coinciding with the diversification of corals and the formation of coastal habitats (fig. 2*B*; Bellwood et al. 2017). More than 60% (~250 species) of lineages dispersed out of CIP into different subareas within the IP. These events mostly occurred around when the IAA rearrangement concluded (~5 Ma; Lohman et al. 2011). Fewer dispersal events (~40% lineages) happened outside the remaining (non-CIP) areas and mostly occurred after the IAA rearrangement (fig. 2*A*). These findings are supported by the cumulative lineage plot over time (fig. 1*B*), which shows that syngnatharian lineages have primarily accrued throughout their history in the IP, particularly within the CIP. Notably, lineages started dispersing to the CIP more frequently after the Tethys Seaway closure (fig. 1*B*). We also observed that syngnatharian lineages tended to disperse at high rates among adjacent areas (fig. 2*A*). Dispersal rates are higher within IP subareas (0.028–0.046) than

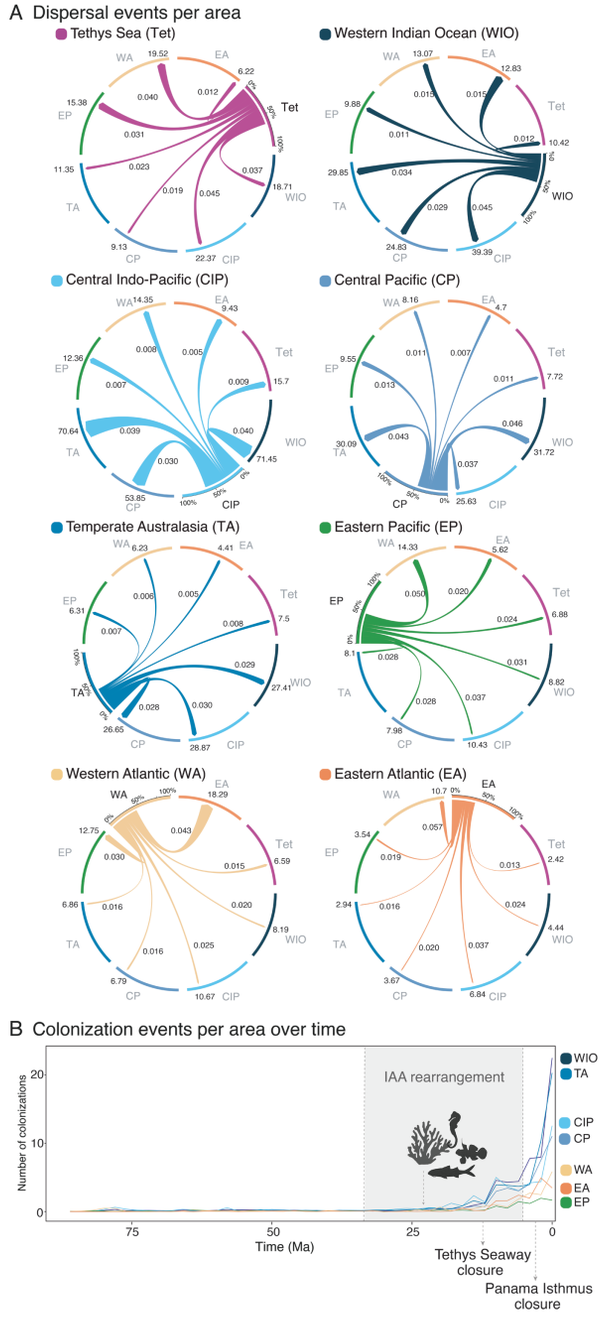

Figure 2: Tempo and mode of dispersal and colonization events between different biogeographic regions. The Indo-Pacific (IP) acts as a center of accumulation for syngnatharian lineages, a process that correlates with the Indo-Australian archipelago (IAA) rearrangement and the expansion of modern coral reef formations. The central Indo-Pacific (CIP) acts as a source (many dispersals outward) of lineages, while the Atlantic, particularly the eastern Atlantic (EA), acts as a sink (relatively higher colonizations). *A*, Chord diagrams for dispersal events outside each region; line width represents the percentage of lineages dispersing from a focal area to the rest of the areas. The total number of lineages dispersed and dispersal rates are depicted outside and inside the diagrams, respectively. *B*, Total number of colonizations per area over time. Note that while the IP has higher total colonizations over time compared with other regions, the relative proportion of colonizing (vs. dispersing) lineages is actually lower than in other basins. For example, the EA has 52 colonizations and 20 outward dispersals, whereas the CIP has 118 colonizations and 244 outward dispersals. For complementary analyses, see figures S10–S16.

between oceanic realms (0.005–0.015). Within the IP, WIO is the region that received the highest number of colonizations (22 independent lineages), followed closely by TA (20), while colonizations into CIP and CP are roughly half of that (11 and 10, respectively). Colonization events over time into the Atl and EP tend to be more recent, mostly concentrated around the closure of the Isthmus of Panama (fig. 2*B*). Fewer lineages have colonized these two realms compared with the IP (fig. 2). Dispersal rates are highest from the EA into the WA (0.057), followed by from the EP into the WA (0.050), and from the WA into the EP (0.030) and EA (0.043). Dispersal rates from these three areas into the IP are overall lower, ranging from 0.016 to 0.037 (fig. 2*A*). At the two extremes, the CIP receives twice as many lineages as it disperses (118 received vs. 244 dispersed), while the EA receives 52 lineages and disperses 20 (fig. 2*A*).

Speciation rates per area over time tend to correlate with major geological and climatic events (fig. 1*C*). We observe three major peaks: one marking the early Tethyan origin of all main (suborder-level) lineages in Syngnatharia (~80 Ma), a second peak within the IP after the PETM (~56 Ma), and a third peak in all areas, mostly after the beginning of the IAA rearrangement (~35 Ma). Thereafter, speciation rates had similar dynamics within each ocean showing a decrease to the present, particularly after the closure of the Isthmus of Panama (2.8 Ma). Finally, extirpation rates across regions are rarely constant over time, although the WA shows higher rates until ~60 Ma (fig. S13). When comparing all of these results with those obtained using the BAYAREA model without the *j* parameter, we find similar patterns (fig. S14), although colonization rates tend to be higher overall when including jump dispersal in the model (fig. S10). Analyses conducted on the alternative tree produced results similar to those obtained from the master tree (figs. S11, S12), except the sequence of events began slightly earlier in MCMCTree analyses (figs. S15, S16).

Diversification Rates among Regions

After accounting for topological and divergence time uncertainties, lineage diversification analyses show no major differences whether using all taxa (323 tips) or after excluding potential instances of taxonomic oversplitting (311 tips; see fig. S17). Thus, here we report the results obtained using

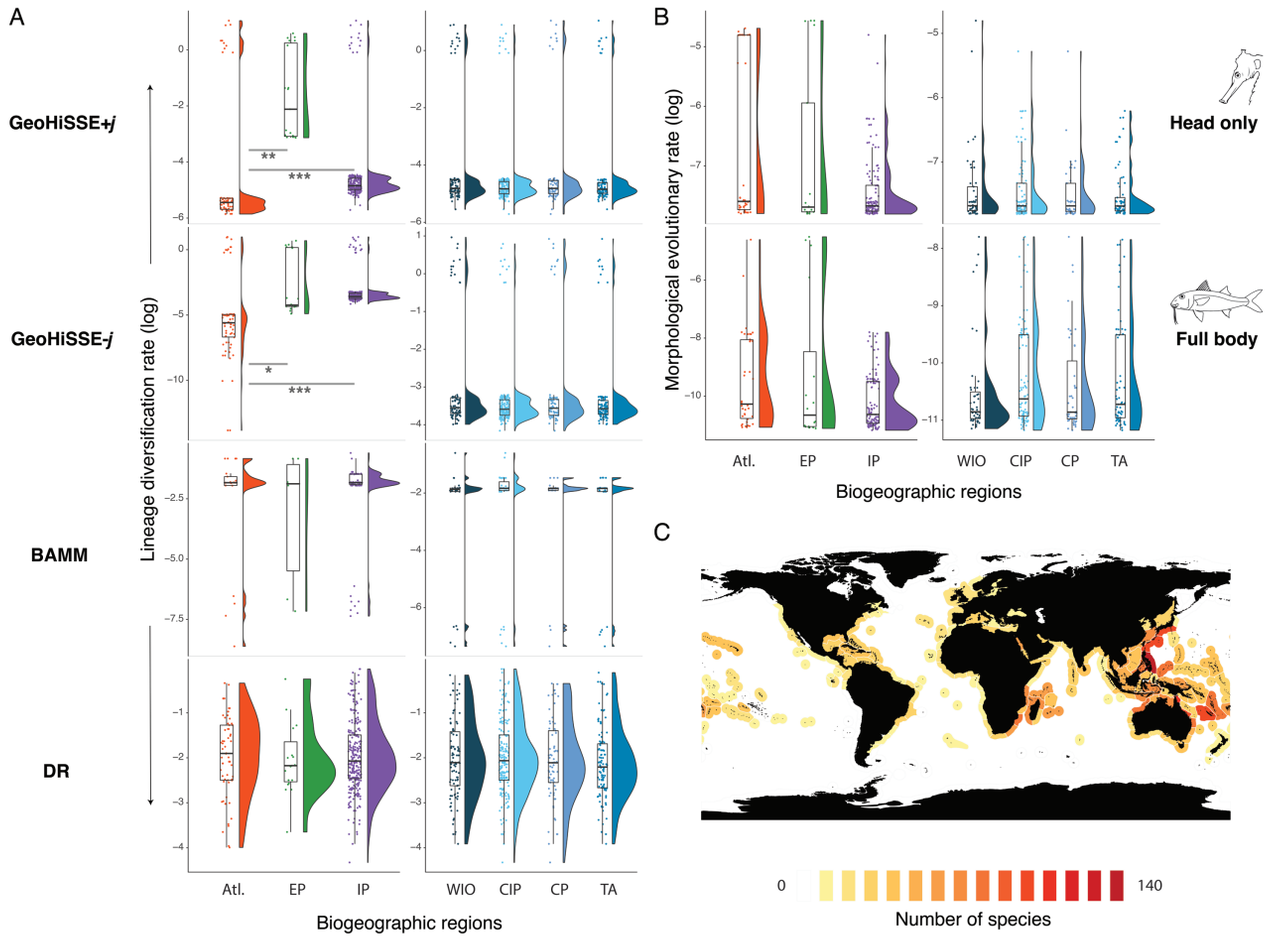

Figure 3: Lineage and morphological diversification rates and species richness across biogeographic regions. The high species richness in the Indo-Pacific (IP) cannot be attributed to rate differences: both rates of lineage diversification and shape evolution are similar across ocean regions, except for GeoHiSSE analyses, which show lower rates in the Atlantic. *A*, Average log-transformed rates of lineage diversification estimated according to three different approaches (GeoHiSSE±*j*, BAMM, and DR) and depicted using rain cloud plots (half-violin plots and boxplots). *B*, Average log-transformed rates of shape evolution estimated in BAMM with phylogenetically corrected principal component scores and depicted using rain cloud plots for both datasets (head-only shape and full-body shape). Points represent mean tip rates for each species. Asterisks indicate statistical significance between regions ($^{*}P \leq .05$; $^{**}P \leq .01$; $^{***}P \leq .001$; see table S6). *C*, Map shows species richness for syngnatharians; colors are proportional to the number of species based on data from Marine Ecoregions of the World. Atl = Atlantic; EP = eastern Pacific; WIO = western Indian Ocean; CIP = central Indo-Pacific; CP = central Pacific; TA = temperate Australasia. For more detailed analyses, see figures S18–S10 and S32–S36.

the complete taxonomic dataset. The CIP, particularly in New Caledonia, Philippines, Taiwan, and Japan, is the region with the highest species richness, while the Atl and EP have the lowest (fig. 3*C*). BAMM and DR analyses show no significant differences in lineage diversification rates across the three major realms (BAMM: $\chi^2 = 0.262$, df = 2, $P = .887$; DR: $\chi^2 = 0.747$, df = 2, $P = .688$) or within the IP subareas (BAMM: $\chi^2 = 5.121$, df = 3, $P = .163$; DR: $\chi^2 = 0.794$, df = 3, $P = .851$; fig. 3*A*; table S6). Uniquely, GeoHiSSE±*j* estimates using model averaging identified the highest rates in the EP (median: 0.12), followed by the IP (0.008), with the lowest in the Atl (0.004; fig. 3*A*). Species with widespread distributions tend to have higher diversification rates based on GeoHiSSE±*j* (figs. 3*A*, S18). Clades that undergo bursts of speciation also exhibit higher rates in GeoHiSSE±*j* and BAMM. Specifically, this pattern is observed in *Syngnathus* lineages within the EP (e.g., the most recent common ancestor [MRCA] of *S. auliscus* and *S. californiensis*) and the Atl (e.g., MRCA of *S. schlegeli* and *S. pelagicus*) regions, consistent with findings reported by Stiller et al. (2022). Additionally, similar trends are observed in *Callionymus* spp. within the IP (e.g., MRCA of *C. valenciennei* and *C. planus*). Using tip-associated rates calculated from GeoHiSSE (+*j*: $\chi^2 = 23.16$, df = 2, $P = 9.36e{-}6$;

$-j$: $\chi^2 = 29.46$, df = 2, $P = 4.01e{-}7$), we find significant differences between Atl and IP ($+j$: $P = 7.6e{-}6$; $-j$: $P = 9.50e{-}8$) and between Atl and EP ($+j$: $P = .003$; $-j$: $P = .047$), whereas all analyses show constant diversification rates within IP subareas (median: ~0.008; $+j$: $\chi^2 = 5.24$, df = 3, $P = .15$; $-j$: $\chi^2 = 5.55$, df = 3, $P = .14$; fig. 3*A*; table S6). At the suborder level, Syngnathoidei ($+j$: $\chi^2 = 16.69$, df = 2, $P = 2.38e{-}4$; $-j$: $\chi^2 = 19.42$, df = 2, $P = 6.06e{-}5$) and Mulloidei ($+j$: $\chi^2 = 11.43$, df = 2, $P = .003$; $-j$: $\chi^2 = 16.87$, df = 2, $P = 2.17e{-}4$) also show major rate differences between Atl and IP ($+j$: $P = 1.3e{-}4$ [Syngnathoidei] and 0.002 [Mulloidei]; $-j$: $P = 2.2e{-}5$ [Syngnathoidei] and $5.1e{-}5$ [Mulloidei]) and between Atl and EP ($+j$: $P = 0.045$ [Syngnathoidei] and 0.034 [Mulloidei]; $-j$: $P = .013$ [Mulloidei]) in GeoHiSSE±*j* analyses (fig. S18; table S6). Other suborders, however, show rate constancy across geographies regardless of the method used (fig. S18). When comparing these results with those obtained using MCMCTree trees, analyses based on all species also show no significant differences among biogeographic regions (fig. S19; table S6). Additionally, diversification rates across all three methods show no significant differences between both sides of the Atl ($\chi^2 = 0.06$–2.75, df = 1, $P = .09$–$.852$; fig. S36). We find significant differences when using MCMCTree trees in the suborder Callionymoidei across the three realms($+j$: $\chi^2 = 19.35$, df = 2, $P = 6.28e{-}5$; $-j$: $\chi^2 = 21.10$, df = 2, $P = 2.62e{-}5$), particularly between the Atl and the EP ($+j$: $P = .008$), between the Atl and the IP ($+j$: $P = 3e{-}5$; $-j$: $P = 1.1e{-}5$), and within the IP subareas ($+j$: $\chi^2 = 11.01$, df = 3, $P = .01$; $-j$: $\chi^2 = 9.79$, df = 3, $P = .02$). Differences were observed between the CIP and the CP in GeoHiSSE+*j* ($P = .040$) and between the CIP and the TA in GeoHiSSE−*j* ($P = .049$), which were not apparent when using RelTime trees (table S6). We also find significance in Mulloidei (BAMM: $\chi^2 = 8.97$, df = 2, $P = .01$; GeoHiSSE+*j*: $\chi^2 = 9.98$, df = 2, $P = .007$; $-j$: $\chi^2 = 7.05$, df = 2, $P = .029$) between the Atl and the IP across all the methods except for DR (BAMM: $P = .024$; GeoHiSSE+*j*: $P = .005$; $-j$: $P = .035$; fig. S20; table S6). Results of DR analyses after accounting for topological incongruences with respect to the Stiller et al. (2022) phylogeny are also similar (fig. S38; table S6).

Morphological Disparity and Rates by Region

Morphospace analyses using both head and body shape datasets show overlap in major realms and within the IP (figs. 4, S21). Head morphology exhibits higher similarity in both morphospace occupation and disparity within IP subareas, particularly between CIP and TA (figs. 4*A*, 5*A*; see app. 2, available on Dryad Digital Repository [https://doi.org/10.5061/dryad.zkh1893gd; Santaquiteria et al. 2024]). Body shape overlap is generally lower than that of head shape (fig. 4*B*; see app. 2). We found that disparity in head morphology (including seahorses) is higher in the IP (0.055) and EP (0.057) than in the Atl (0.048; fig. 5*A*). However, disparity in body morphology is higher in the Atl (0.039) and EP (0.045) than in the IP (0.030; fig. 5*B*). Disparity among subareas within the IP is rather similar, although head shape has higher disparity than body morphology (head: WIO [0.058], CP [0.058], CIP [0.056], TA [0.056]; body: WIO [0.034], TA [0.032], CIP [0.028], CP [0.028]; fig. 5). However, within the Atl the opposite pattern is observed (head: EA [0.050], WA [0.051]; body: EA [0.040], WA [0.041]; fig. S36]. Suborder-level analyses reveal idiosyncratic patterns of disparity across biogeographic regions that do not necessarily reflect results for Syngnatharia as a whole (fig. 6). These findings hold when using different tree sources (RelTime and MCMCTree) and PC versus pPC scores (figs. 6, S26, S27).

Multivariate disparity through time analyses indicate that a significant proportion of morphological variation originated early in the history of Syngnatharia (~87–78 Ma), followed by a steady reduction in disparity during most of the Cenozoic with a small peak to the present (figs. 5, S28). For head-only morphology, models with a shift in evolutionary process over time, specifically BMOUi and EBOUi models, were best supported (AICw = 0.61 and 0.36, respectively; fig. S29). Most of the analyses of full-body morphology favored BM (AICw = 0.82–0.96; fig. S30). Morphospace clustering tends to differentiate suborder- or family-level lineages, which could be indicative of multiple adaptive peaks (fig. S31). Morphological evolutionary rates are similar across major realms (head: median, ~0.0005; body: $3.4e{-}5$; EP and IP: $2.4e{-}5$; fig. 3*B*). We also observe these rates being similar within subareas of the IP (head: WIO, CP, CIP, and TA [~0.0003]; body: WIO and CP [$1.9e{-}5$], CIP [$2.4e{-}5$], TA [$2.2e{-}5$]; fig. 3*B*] and the Atl (head: EA [0.003], WA [0.002]; body: EA [0.0003], WA [0.0006]; fig. S36]. No significant differences in rates were found between biogeographic regions overall (table S7; figs. 3, S32–S36), except within Syngnathoidei ($\chi^2 = 9.75$, df = 2, $P = .007$), with significant differences in head-only morphology between the Atl and the IP ($P = .011$), a result mostly driven by the high morphological rates in the Atl for the genus *Syngnathus* (figs. 6, S32; table S7). We observe similar results using uncorrected PC scores, with significance in head-only morphology (within IP: $\chi^2 = 11.66$, df = 3, $P = .008$), between WIO and TA subareas ($P = .035$), and for full-body morphology in Syngnathoidei (between realms: $\chi^2 = 9.54$, df = 2, $P = .008$) between the Atl and IP ($P = .011$; fig. S33; table S7). Analyses using MCMCTree trees are largely similar (fig. S34), with PC scores showing

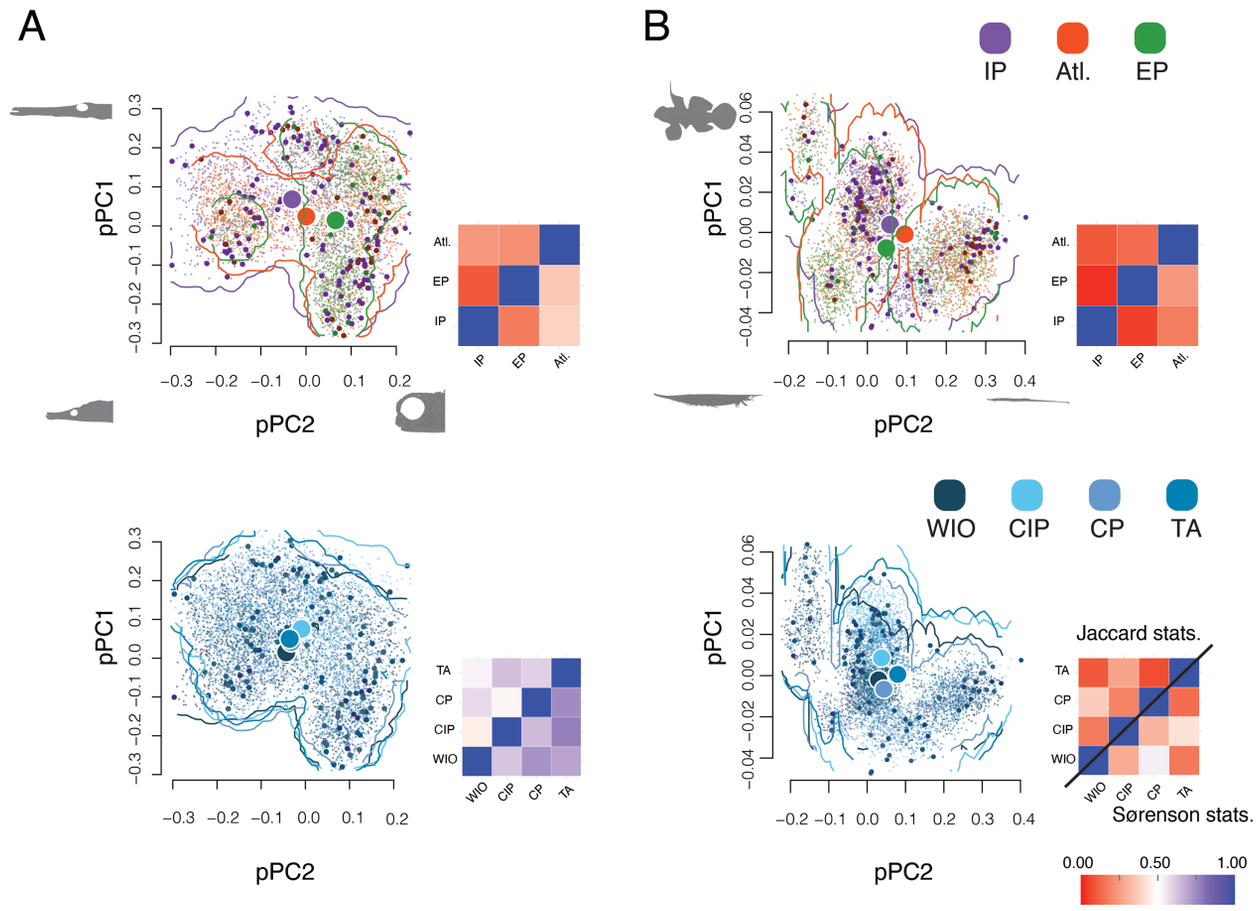

Figure 4: Patterns of morphospace occupation (hypervolumes) for head-only (*A*) and full-body (*B*) datasets, showing greater overlap within Indo-Pacific (IP) regions. The large circles represent hypervolume centroids of the different biogeographic regions. Dark-colored points represent each observed species by area, while light-colored points are uniformly distributed within the hypervolume inferred by the single-value vector machine learning. Lines delineate morphospace occupation. Note that while hypervolumes are plotted in two dimensions for visualization purposes (phylogenetically corrected PCs 1 and 2), morphospace overlap/similarity is calculated according to four-dimensional (head-only) and six-dimensional (full-body) hypervolume overlap statistics using Jaccard (above the diagonal of the heat map) and Sørenson (below the diagonal of the heat map) indexes. Colder and warmer colors correspond to higher and lower overlap between areas, respectively. Atl = Atlantic; EP = eastern Pacific; WIO = western Indian Ocean; CIP = central Indo-Pacific; CP = central Pacific; TA = temperate Australasia. For complementary analyses, see figures S21–S25.

significance across the three main realms in body morphology ($\chi^2 = 6.04$, df $= 2$, $P = .049$) between the Atl and the EP ($P = .041$) and between the Atl and the IP ($P = .0002$) for Syngnathoidei (fig. S35; table S7).

Discussion

In this study, we conducted integrative comparative analyses within a robust phylogenomic framework to test three hypotheses that may explain the high species richness of syngnatharians in the IP and its correspondence with morphological disparity. We found the strongest support for the center of accumulation (higher colonization events to the IP) and time for speciation (earlier colonization to the IP providing lineages with more time to diversify) hypotheses and low support for the center of origin hypothesis, as lineage diversification rates are not significantly higher in the IP compared with the less diverse Atl and the EP. The higher species richness of the IP today for syngnatharians is thus attributed to its relatively earlier colonization (after Tethys reorganization), with diversification rates near the present remaining constant across all three realms. These colonizations also facilitated the spread of body plans to different regions, explaining the high overlap in morphological disparity in syngnatharians across oceans. This similarity is not the result of independent evolution of the same body plans within each biogeographic region but rather due to

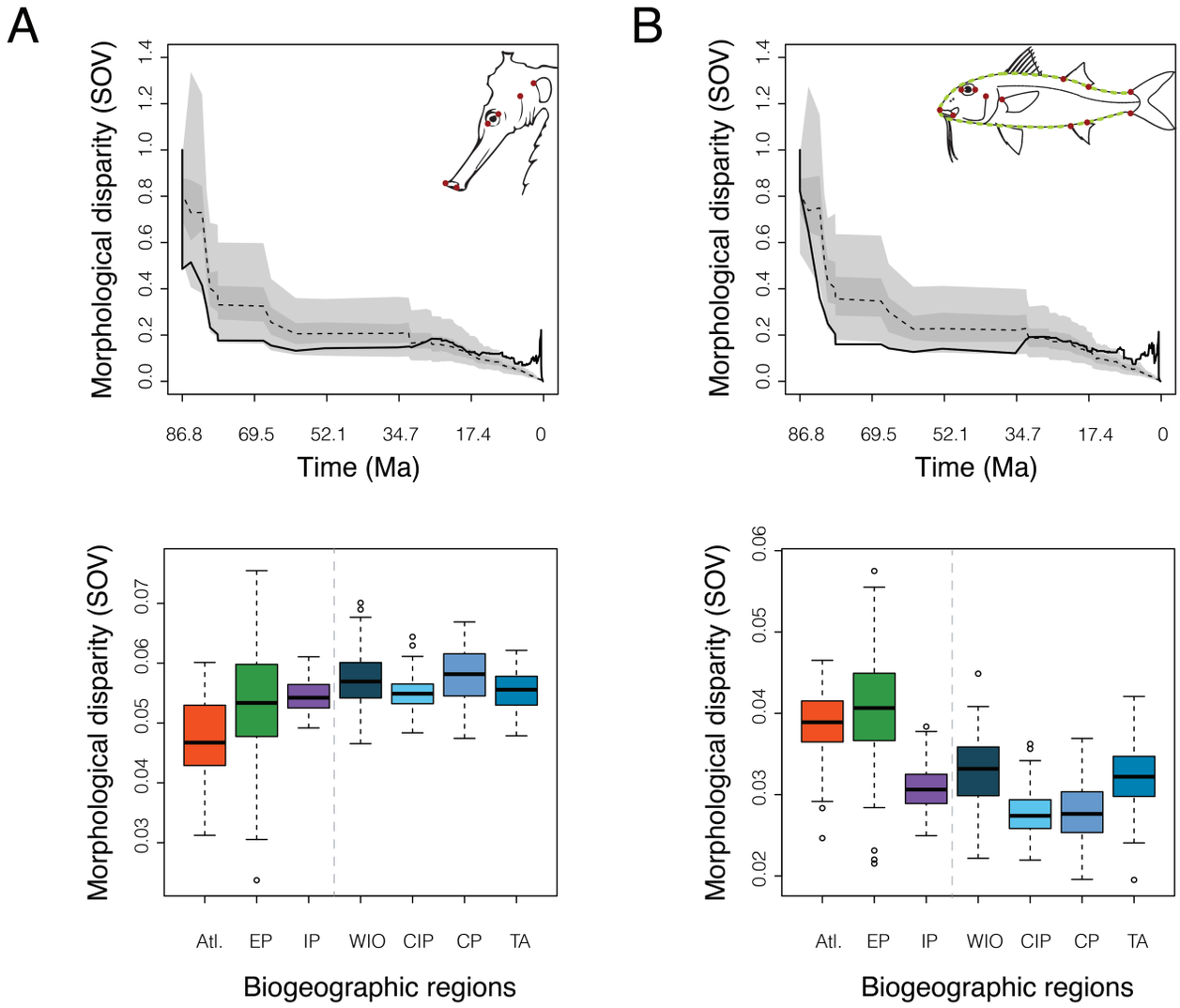

Figure 5: Disparity across regions and through time for syngnatharians estimated using sum of variances (SOV) for head-only (*A*) and full-body (*B*) datasets. Disparity through time (DTT) analyses show an early burst of shape evolution, while patterns of contemporary disparity across regions are relatively similar, except for full-body disparity, which is higher in the Atlantic (Atl) and eastern Pacific (EP). The solid line in the DTT plots represents observed disparity. The dashed line represents the mean of 100 Brownian motion simulations, the dark gray area shows the distribution of simulations within the 25%–75% percentiles, and the light gray area denotes the 2.5%–97.5% percentiles. Fish illustrations denote the landmark schemes used for two-dimensional geometric morphometric analyses, with red points representing homologous landmarks and green dotted lines representing the semilandmarks. IP = Indo-Pacific; WIO = western Indian Ocean; CIP = central Indo-Pacific; CP = central Pacific; TA = temperate Australasia. For complementary analyses, see figures S26–S31.

an early burst of shape evolution that likely occurred within the Tethys. Thus, our results show that the generation of morphological disparity was largely decoupled from species richness patterns. These findings align with trends observed at larger phylogenetic scales in numerous families of reef fishes, emphasizing the significance of time and colonization in shaping regional species richness (Miller et al. 2018), along with the presence of analogous functional traits across an oceanic longitudinal gradient (Mouillot et al. 2014; McLean et al. 2021).

The time for speciation and center of accumulation hypotheses also find support across various taxa. For example, terrestrial turtles in the eastern part of North America (Stephens and Wiens 2003), freshwater fishes in the Amazon basin in South America (García-Andrade et al. 2023), and, on a smaller scale, endemic plants in

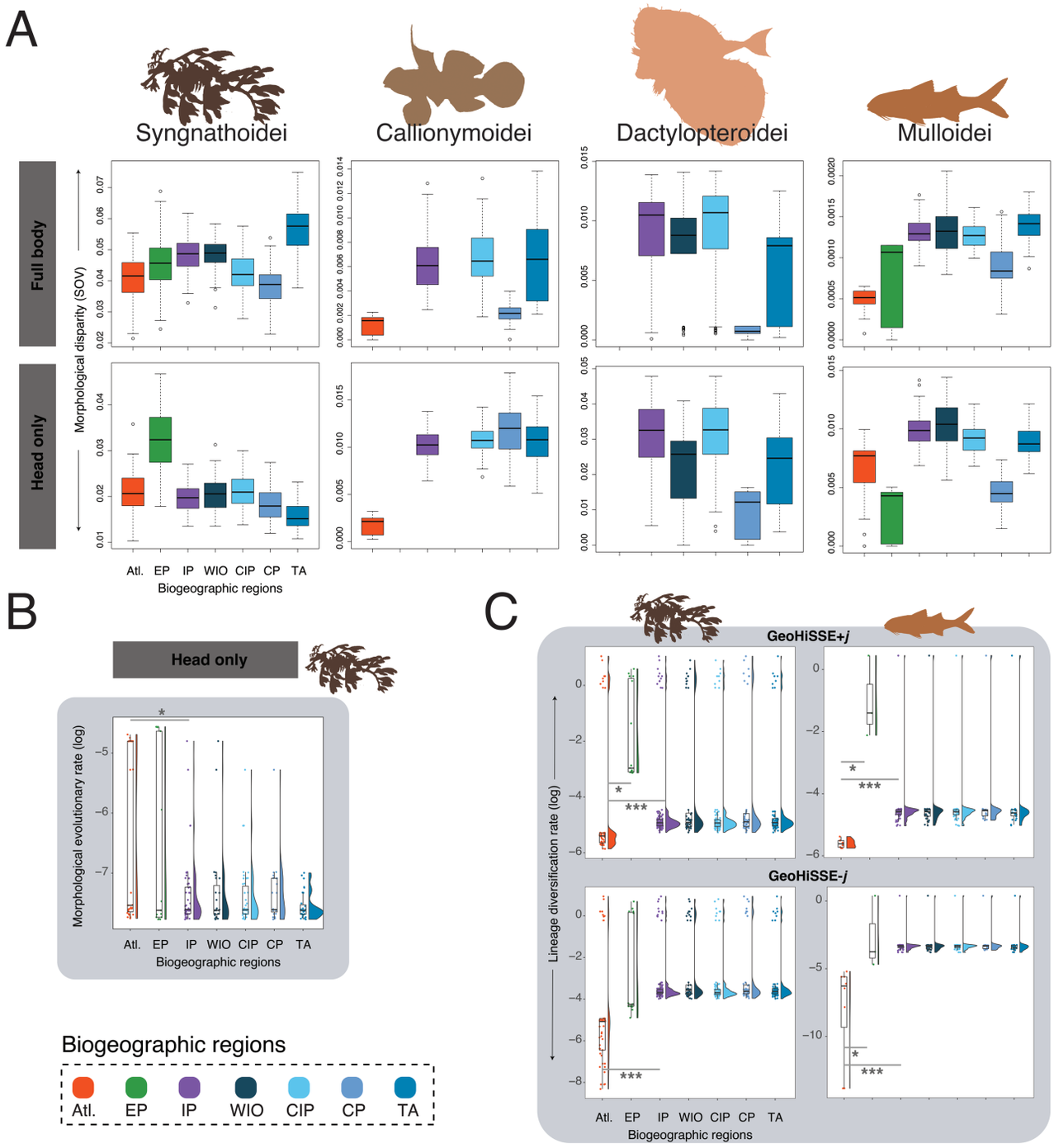

Figure 6: Suborder-level analyses across regions, showing only significant results obtained. *A*, Boxplots illustrating morphological disparity estimated using the sum of variances (SOV). *B*, Morphological evolutionary rates (average log transformed) of head-only evolution estimated in BAMM with phylogenetically corrected principal component scores. *C*, Lineage diversification rates (average log transformed) estimated in GeoHiSSE±*j*. Points in the rain cloud plots in *B* and *C* represent mean tip rates for each species. Asterisks indicate statistical significance between regions (*$P \leq .05$; ***$P \leq .001$. See tables S6 and S7). Note that disparity cannot be calculated for biogeographic regions with fewer than three species (e.g., Callionymoidei in eastern Pacific [EP], Dactylopteroidei in Atlantic [Atl]). IP = Indo-Pacific; WIO = western Indian Ocean; CIP = central Indo-Pacific; CP = central Pacific; TA = temperate Australasia. For all other analyses, including nonsignificant ones, see figures S18–S20, S26, S27, and S31–S36.

Cape Town in the Greater Cape Floristic Region of South Africa (Cowling et al. 2017), all exhibit higher species richness in these regions because of early and greater number of colonizations into these areas. Similarly, our results indicate that the timing of colonizations significantly contributes to the high species richness of IP syngnatharians, paralleling trends seen across all marine reef fishes (Miller et al. 2018). After colonizing the IP region from the Tethys Sea, syngnatharian lineages underwent in situ speciation, coinciding with the PETM paleoclimatic event at ~56 Ma, during which global warming and ocean acidification occurred (McInerney and Wing 2011). The fossil record shows that this event also led to increased extinction in some marine fish groups (Arcila and Tyler 2017), potentially enabling syngnatharians to expand into novel niches. The establishment of tropical reefs primarily composed of scleractinian corals around the same period (Wallace and Rosen 2006; Mihaljević et al. 2014; Santodomingo et al. 2015) might also have helped in accelerating speciation. The early Eocene environmental conditions, which encompassed coastal biomes like seagrasses, potentially facilitated the diversification and rapid expansion of different reef fish clades into new ecological niches (e.g., Bellwood 2003; Wainwright et al. 2012). In the Miocene (23 Ma on), with the rearrangement of the IAA (which is part of the CIP), a recognized hot spot for marine reef fishes (Renema et al. 2008; Leprieur et al. 2016), major reef fish groups, including syngnatharians, wrasses, and damselfishes, began diversifying across various regions globally, particularly flourishing within the CIP region (Cowman and Bellwood 2011; Siqueira et al. 2020). This period also saw the expansion of modern coral reef formations mainly by acroporids (e.g., Cowman and Bellwood 2011; Siqueira et al. 2021), zooxanthellate corals, and gastropods (Williams and Duda 2008). Consequently, coral reefs have played a dual role as both evolutionary cradles and ecological refuges for a wide array of tropical marine lineages influencing species richness (Bellwood et al. 2005, 2015).

The lack of barriers or the presence of soft barriers along a group's range usually generates a peak of high species richness to the center of the geographical domain (middomain effect; Colwell et al. 2004). It is also possible that syngnatharian diversity, and marine vertebrate and invertebrate diversity in general, is highest in the CIP because of its central position within the IP (e.g., Tittensor et al. 2010; Edgar et al. 2017). This pattern may also be explained by species that occupy multiple regions (widespread range) within the IP, potentially supporting the center of overlap hypothesis (not tested in this study; Woodland 1983). Lineages originating in this region exhibit high dispersal rates to surrounding areas, serving as a source for the rest of the IP. However, because of stronger dispersal barriers across oceans, most lineages that colonized either side of the Atl and the EP tended to remain within their respective regions. This explains the low number of dispersal events and rates observed out of these regions. Consequently, the Atl and EP regions have generally functioned as sinks. These regions have also experienced higher extirpation rates compared with the IP, primarily because of a series of geologic and climatic events—the closure of the Tethys Seaway and the rise of the Isthmus of Panama and the Middle Miocene Climate Transition—that caused environmental changes, including sea level and temperature fluctuations, ocean current circulation oscillation, salinity variations, and shifts in primary productivity (Leprieur et al. 2016; Steinthorsdottir et al. 2021). These patterns align with some results from our lineage diversification rate analyses using GeoHiSSE±*j*, which indicate higher net diversification rates in the IP compared with the Atl. It is noteworthy, however, that this finding might not be a result of elevated in situ speciation in the IP but rather due to the higher extirpation rates in the Atl as explained above.

Along the longitudinal axis, patterns of species richness are decoupled from morphological disparity and rates of head and body shape evolution, with species-rich areas exhibiting similar disparity and rates of morphological evolution as less specious areas. This contrasts with a recent study in fishes that observed a negative correlation between these factors along a latitudinal gradient, with species-poor high latitudes exhibiting higher disparity and rates of body shape evolution than more diverse equatorial latitudes (Burns et al. 2024). Shallow reefs have been formed through consistent environmental and ecological pressures generating most body plans in all of the biogeographic regions (McLean et al. 2021). Despite significant differences in species richness between realms and considering the evolutionary history of syngnatharian clades and reef fishes in general, these patterns suggest that functional space richness is similar across regions, indicating shared functional roles (Mouillot et al. 2014; McLean et al. 2021).

Although a few body plans in Syngnatharia are restricted to particular regions—for example, the bat shape of the seamoths, the macroalgae- or octocoral-like appearance of ghost pipefishes, or the camouflage-mimicking seaweed morphology of sea dragons in the IP—what characterizes the trajectory of morphological evolution in this group is an early diversification in body plans before the Cretaceous-Palaeogene (K-Pg) mass extinction event. It was during this period (90–66 Ma) that acanthomorph fishes displayed an overall expansion in their general head shape (Sallan and Friedman 2012), despite the low complexity of reefs at this time (Kiessling 2009). After the K-Pg mass extinction event, we observe morphospace clustering in multiple regions of the morphospace, roughly aligning with suborder-level clades within syngnatharians (Nash et al. 2022), indicating the emergence of specializations,

particularly within the IP. These specializations may have arisen following the extinction of competitors (e.g., Friedman 2010; Wainwright and Longo 2017; Duarte-Ribeiro et al. 2018).

Uncertainties in Macroevolutionary Inferences and Study Caveats

Implementing exhaustive and integrative phylogenomic approaches to account for topological, divergence times, and method uncertainty is crucial in macroevolutionary analyses (e.g., Henao Diaz et al. 2019; Rincon-Sandoval et al. 2020; Goswami et al. 2022). We utilized 28 trees from independent gene subsets to address uncertainties in historical biogeography, lineage diversification, and morphological evolution. In biogeographic analyses, dating methods (Schwartz and Mueller 2010) and the jump dispersal parameter (Ree and Sanmartín 2018; Matzke 2022) had significant impacts on speciation, extinction, and colonization patterns. Diversification rate analyses showed varied outcomes depending on method, influencing interpretations. For example, BAMM (parametric) and DR (nonparametric) tip-rate analyses fail to reject the time for speciation hypothesis, as they identify no rate differences across oceans, while GeoHiSSE (state-dependent diversification) supports the center of origin hypothesis. As a result, we use caution in our interpretations by considering incongruent results. Morphological analyses indicated consistent results with pPC and PC scores, but dating methods influenced the best-fit model selection for body plans. While tree uncertainty had minimal impact in comparative analyses, morphological evolution varied significantly across trees (fig. S30), cautioning against reliance on single-tree estimates. Despite these insights, single-tree approaches are still common in estimating lineage diversification rates (e.g., Feng et al. 2017; Xing and Ree 2017). We advocate for using multiple trees and diverse methodologies to comprehensively address uncertainty (e.g., Economo et al. 2018; Title and Rabosky 2019). The age of Syngnatharia may influence observed patterns, warranting exploration in younger clades (Clarke 2021; Miller et al. 2021; Nash et al. 2022; Diamond and Roy 2023). Morphological disparity varied among suborders; for instance, the CP exhibited lower disparity in Callionymoidei, Dactylopteroidei, and Mulloidei, while the EP showed higher disparity in Syngnathoidei (fig. S21).

Despite sampling nearly 50% of syngnatharian species across regions and employing multiple approaches, we acknowledge limitations in the reliability of phylogenetic extirpation estimates (Rabosky 2010; Beaulieu and O'Meara 2015). Disparities in sampling across oceans, speciation rate variations, and taphonomic biases (distortions in the fossil record) in our phylogenies could have influenced rate estimations and biogeographic patterns. For instance, reef fishes are well represented in the Eocene Bolca Lagerstätten (western Tethys Sea; Bellwood 1996; Friedman and Carnevale 2018), contrasting with scarce Atl fossils. Notable exceptions in the Atl include fossils from the Tenejapa-Lacandón Formation in Palenque, Mexico, dating back to 63 Ma (Cantalice et al. 2022). Other limitations of our study include the potential underestimation of morphological disparity because of the absence of semilandmarks on fins or ornaments (e.g., leaflike protrusions in leafy sea dragons) and the inability to include seahorse specimens with bent structures in full-body shape analyses. Capturing the globular shapes of syngnatharian species using two-dimensional images is also challenging. Future work should prioritize collecting computed tomography scan data for three-dimensional geometric morphometric analyses (e.g., Buser et al. 2018; Evans et al. 2023). While morphology can indicate niche use, direct assessments of ecology, function, or physiology could offer deeper insights into niche-related evolution and its impact on group diversification in relation to historical events. Future studies should explore additional biotic variables, such as different functional traits, alongside environmental factors, such as sea level, temperature, and primary productivity.

Conclusions

We find that the high diversity of syngnatharian species in the IP is primarily due to older colonizations followed by in situ speciation in the Paleocene, shortly after the PETM, and lineage accrual in the Miocene at the onset of the IAA rearrangement. In contrast, the EP and the Atl feature lower regional diversities because of more recent colonization and diversification onset, with lineages in these regions mostly accruing during the Miocene. Overall, these findings best support the time for speciation and center of accumulation hypotheses. We also observe both disparity and rates of morphological evolution to be similar across areas, with clade-specific variations. Our results reveal uncorrelated species richness and morphological disparities in syngnatharians along their longitudinal gradient. Instead, they demonstrate that a considerable portion of syngnatharian morphological variation emerged early in their evolutionary history in the Tethys Sea, followed by a gradual reduction in subclade disparity punctuated by the origin of morphospace clustering, especially in head morphology. This study advances our understanding of the evolutionary processes that have shaped the diversity and morphology of marine fishes in general and syngnatharians in particular, underscoring the importance of considering multiple factors affecting historical biogeographic and macroevolutionary inferences.

Acknowledgments

We thank S. Raredon (Smithsonian National Museum of Natural History) for providing assistance with photographs. Bioinformatic analyses were facilitated by the University of Oklahoma Supercomputing Center for Education and Research. We are grateful to K. Marske (University of Oklahoma) and D. Moen (Oklahoma State University) for their helpful comments on the manuscript.

Statement of Authorship

A.S., R.B.-R., D.A., and M.W.W. conceptualized the study. A.S. and R.B.-R. designed the methodological approach. A.S., E.M.T., C.d.R.P.-M., and G.C. collected the data. A.S. analyzed the data with assistance from E.C.M. A.S. and U.R.-P. created the figures. A.S. and R.B.-R. wrote the manuscript and supplemental material, with G.C. and U.R.-P. contributing to portions of the supplementary text. All authors reviewed and edited the manuscript.

Data and Code Availability

All data and code are available in the Dryad Digital Repository (https://doi.org/10.5061/dryad.zkh1893gd; Santaquiteria et al. 2024).

Literature Cited

Adams, D. C., M. L. Collyer, A. Kaliontzopoulou, and E. Baken. 2021. geomorph: geometric morphometric analyses of 2D and 3D landmark data. R package version 3.3.2. https://cran.r-project.org/package=geomorph.

Arcila, D., and J. C. Tyler. 2017. Mass extinction in tetraodontiform fishes linked to the Palaeocene-Eocene thermal maximum. Proceedings of the Royal Society B 284:20171771.

Barber, P. H., and D. R. Bellwood. 2005. Biodiversity hotspots: evolutionary origins of biodiversity in wrasses (Halichoeres: Labridae) in the Indo-Pacific and New World tropics. Molecular Phylogenetics and Evolution 35:235–253.

Beaulieu, J. M., and B. C. O'Meara. 2015. Extinction can be estimated from moderately sized molecular phylogenies. Evolution 69:1036–1043.

Bellwood, D. R. 1996. The Eocene fishes of Monte Bolca: the earliest coral reef fish assemblage. Coral Reefs 15:11–19.

———. 2003. Origins and escalation of herbivory in fishes: a functional perspective. Paleobiology 29:71–83.

Bellwood, D. R., C. H. R. Goatley, and O. Bellwood. 2017. The evolution of fishes and corals on reefs: form, function and interdependence. Biological Reviews 92:878–901.

Bellwood, D. R., C. Goatley, and P. F. Cowman. 2015. The evolution of fishes on coral reefs: fossils, phylogenies, and functions. Pages 55–63 *in* C. Mora, ed. Ecology of fishes on coral reefs. Cambridge University Press, Cambridge.

Bellwood, D. R., T. P. Hughes, S. R. Connolly, and J. Tanner. 2005. Environmental and geometric constraints on Indo-Pacific coral reef biodiversity. Ecology Letters 8:643–651.

Blonder, B., C. B. Morrow, B. Maitner, D. J. Harris, C. Lamanna, C. Violle, B. J. Enquist, and A. J. Kerkhoff. 2018. New approaches for delineating *n*-dimensional hypervolumes. Methods in Ecology and Evolution 9:305–319.

Bowen, B. W., L. A. Rocha, R. J. Toonen, and S. A. Karl. 2013. The origins of tropical marine biodiversity. Trends in Ecology and Evolution 28:359–366.

Bray, D. J., and M. F. Gomon. 2021. Fishes of Australia. Museums Victoria/OzFishNet, Melbourne. http://fishesofaustralia.net.au/.

Briggs, J. C. 1974. Marine zoogeography. McGraw-Hill, New York.

Burns, M. D., S. T. Friedman, K. A. Corn, O. Larouche, S. A. Price, P. C. Wainwright, and E. D. Burress. 2024. High-latitude ocean habitats are a crucible of fish body shape diversification. Evolution Letters 8:669–679.

Buser, T. J., B. L. Sidlauskas, and A. P. Summers. 2018. 2D or not 2D? testing the utility of 2D vs. 3D landmark data in geometric morphometrics of the sculpin subfamily Oligocottinae (Pisces; Cottoidea). Anatomical Record 301:806–818.

Caetano, D. S., B. C. O'Meara, and J. M. Beaulieu. 2018. Hidden state models improve state-dependent diversification approaches, including biogeographical models. Evolution 72:2308–2324.

Cantalice, K. M., J. Alvarado-Ortega, D. R. Bellwood, and A. C. Siqueira. 2022. Rising from the ashes: the biogeographic origins of modern coral reef fishes. BioScience 72:769–777.

Clarke, J. T. 2021. Evidence for general size-by-habitat rules in actinopterygian fishes across nine scales of observation. Ecology Letters 24:1569–1581.

Clavel, J., G. Escarguel, and G. Merceron. 2015. mvMORPH: an R package for fitting multivariate evolutionary models to morphometric data. Methods in Ecology and Evolution 6:1311–1319.

Colwell, R. K., C. Rahbek, and N. J. Gotelli. 2004. The mid-domain effect and species richness patterns: what have we learned so far? American Naturalist 163:E1–E23.

Cowling, R. M., P. L. Bradshaw, J. F. Colville, and F. Forest. 2017. Levyns' law: explaining the evolution of a remarkable longitudinal gradient in Cape plant diversity. Transactions of the Royal Society of South Africa 72:184–201.

Cowman, P. F., and D. R. Bellwood. 2011. Coral reefs as drivers of cladogenesis: expanding coral reefs, cryptic extinction events, and the development of biodiversity hotspots. Journal of Evolutionary Biology 24:2543–2562.

Crouch, N. M. A., and D. Jablonski. 2023. Is species richness mediated by functional and genetic divergence? a global analysis in birds. Functional Ecology 37:125–138.

Diamond, J., and D. Roy. 2023. Patterns of functional diversity along latitudinal gradients of species richness in eleven fish families. Global Ecology and Biogeography 32:450–465.

Ding, W. N., R. H. Ree, R. A. Spicer, and Y. W. Xing. 2020. Ancient orogenic and monsoon-driven assembly of the world's richest temperate Alpine flora. Science 369:578–581.

dos Reis, M., and Z. Yang. 2019. Bayesian molecular clock dating using genome-scale datasets. Methods in Molecular Biology 1910:309–330.

Drury, J. P., J. Clavel, J. A. Tobias, J. Rolland, C. Sheard, and H. Morlon. 2021. Tempo and mode of morphological evolution are decoupled from latitude in birds. PLoS Biology 19:1–28.

Duarte-Ribeiro, E., A. M. Davis, R. A. Rivero-Vega, G. Ortí, and R. Betancur. 2018. Post-Cretaceous bursts of evolution along the benthic-pelagic axis in marine fishes. Proceedings of the Royal Society B 285:20182010.

Dupin, J., N. J. Matzke, T. Särkinen, S. Knapp, R. G. Olmstead, L. Bohs, and S. D. Smith. 2017. Bayesian estimation of the global biogeographical history of the Solanaceae. Journal of Biogeography 44:887–899.

Eastman, J. M., L. J. Harmon, and D. C. Tank. 2013. Congruification: support for time scaling large phylogenetic trees. Methods in Ecology and Evolution 4:688–691.

Economo, E. P., N. Narula, N. R. Friedman, M. D. Weiser, and B. Guénard. 2018. Macroecology and macroevolution of the latitudinal diversity gradient in ants. Nature Communications 9:1–8.

Edgar, G. J., T. J. Alexander, J. S. Lefcheck, A. E. Bates, S. J. Kininmonth, R. J. Thomson, J. E. Duffy, et al. 2017. Abundance and local-scale processes contribute to multi-phyla gradients in global marine diversity. Science Advances 3:e1700419.

Evans, K. M., O. Larouche, S. M. Gartner, R. E. Faucher, S. G. Dee, and M. W. Westneat. 2023. Beaks promote rapid morphological diversification along distinct evolutionary trajectories in labrid fishes (Eupercaria: Labridae). Evolution 77:2000–2014.

Feng, Y.-J., D. C. Blackburn, D. Liang, D. M. Hillis, D. B. Wake, D. C. Cannatella, and P. Zhang. 2017. Phylogenomics reveals rapid, simultaneous diversification of three major clades of Gondwanan frogs at the Cretaceous-Paleogene boundary. Proceedings of the National Academy of Sciences of the USA 114:E5864–E5870.

Friedman, M. 2010. Explosive morphological diversification of spiny-finned teleost fishes in the aftermath of the end-Cretaceous extinction. Proceedings of the Royal Society B 277:1675–1683.

Friedman, M., and G. Carnevale. 2018. The Bolca Lagerstätten: shallow marine life in the Eocene. Journal of the Geological Society 175:569–579.

Froese, R., and D. Pauly. 2021. FishBase. https://www.fishbase.org.au/v4.

Gaboriau, T., C. Albouy, P. Descombes, D. Mouillot, L. Pellissier, and F. Leprieur. 2019. Ecological constraints coupled with deep-time habitat dynamics predict the latitudinal diversity gradient in reef fishes. Proceedings of the Royal Society B 286:20191506.

García-Andrade, A. B., P. A. Tedesco, J. D. Carvajal-Quintero, A. Arango, F. Villalobos, L. D. M. Evolutiva, R. D. B. Evolutiva, et al. 2023. Same process, different patterns: pervasive effect of evolutionary time on species richness in freshwater fishes. Proceedings of the Royal Society B 290:20231066.

Garland, T., and A. R. Ives. 2000. Using the past to predict the present: confidence intervals for regression equations in phylogenetic comparative methods. American Naturalist 155:346–364.

Goswami, A. A., E. Noirault, E. J. Coombs, and J. Clavel. 2022. Attenuated evolution of mammals through the Cenozoic. Science 378:277–383.

Guillerme, T. 2018. dispRity: a modular R package for measuring disparity. Methods in Ecology and Evolution 9:1755–1763.

Henao Diaz, L. F., L. J. Harmon, M. T. C. Sugawara, E. T. Miller, and M. W. Pennell. 2019. Macroevolutionary diversification rates show time dependency. Proceedings of the National Academy of Sciences of the USA 116:7403–7408.

Hipsley, C. A., D. B. Miles, and J. Müller. 2014. Morphological disparity opposes latitudinal diversity gradient in lacertid lizards. Biology Letters 10:20140101.

Jablonski, D., R. Kaustuv, and J. W. Valentine. 2006. Out of the tropics: evolutionary diversity gradient. Science 314:102–106.

Jetz, W., G. H. Thomas, J. B. Joy, K. Hartmann, and A. O. Mooers. 2012. The global diversity of birds in space and time. Nature 491:444–448.

Kiessling, W. 2009. Geologic and biologic controls on the evolution of reefs. Annual Review of Ecology, Evolution, and Systematics 40:173–192.

Kissling, W. D., C. H. Sekercioglu, and W. Jetz. 2012. Bird dietary guild richness across latitudes, environments and biogeographic regions. Global Ecology and Biogeography 21:328–340.

Kulbicki, M., V. Parravicini, D. R. Bellwood, E. Arias-Gonzàlez, P. Chabanet, S. R. Floeter, A. Friedlander, et al. 2013. Global biogeography of reef fishes: a hierarchical quantitative delineation of regions. PLoS ONE 8:e81847.

Ladd, H. S. 1960. Origin of the Pacific Island molluscan fauna. American Journal of Science 258A:137–150.

Lawson, A. M., and J. T. Weir. 2014. Latitudinal gradients in climatic-niche evolution accelerate trait evolution at high latitudes. Ecology Letters 17:1427–1436.

Leprieur, F., P. Descombes, T. Gaboriau, P. F. Cowman, V. Parravicini, M. Kulbicki, C. J. Melian, et al. 2016. Plate tectonics drive tropical reef biodiversity dynamics. Nature Communications 7:11461.

Lohman, D. J., M. de Bruyn, T. Page, K. von Rintelen, R. Hall, P. K. L. Ng, H.-T. Shih, et al. 2011. Biogeography of the Indo-Australian archipelago. Annual Review of Ecology, Evolution, and Systematics 42:205–226.

Longo, S. J., B. C. Faircloth, A. Meyer, M. W. Westneat, M. E. Alfaro, and P. C. Wainwright. 2017. Phylogenomic analysis of a rapid radiation of misfit fishes (Syngnathiformes) using ultraconserved elements. Molecular Phylogenetics and Evolution 113:33–48.

López-Martínez, A. M., S. Magallón, M. von Balthazar, J. Schönenberger, H. Sauquet, and M. Chartier. 2024. Angiosperm flowers reached their highest morphological diversity early in their evolutionary history. New Phytologist 241:1348–1360.

Matzke, N. J. 2013. BioGeoBEARS: BioGeography with Bayesian (and likelihood) evolutionary analysis in R scripts. R package version 0.2.

———. 2019. Run BioGeoBEARS on multiple trees. https://github.com/nmatzke/BioGeoBEARS/blob/master/R/BioGeoBEARS_on_multiple_trees_v1.R.

———. 2022. Statistical comparison of DEC and DEC+J is identical to comparison of two ClaSSE submodels, and is therefore valid. Journal of Biogeography 49:1805–1824.

McInerney, F. A., and S. L. Wing. 2011. The Paleocene-Eocene thermal maximum: a perturbation of carbon cycle, climate, and biosphere with implications for the future. Annual Review of Earth and Planetary Sciences 39:489–516.

McLean, M., R. D. Stuart-smith, S. Villéger, A. Auber, and G. J. Edgar. 2021. Trait similarity in reef fish faunas across the world's oceans. Proceedings of the National Academy of Sciences of the USA 118:e2012318118.

Mihaljević, M., W. Renema, K. Welsh, and J. M. Pandolfi. 2014. Eocene-Miocene shallow-water carbonate platforms and increased habitat diversity in Sarawak, Malaysia. Palaios 29:378–391.

Miller, E. C., K. T. Hayashi, D. Song, and J. J. Wiens. 2018. Explaining the ocean's richest biodiversity hotspot and global patterns of fish diversity. Proceedings of the Royal Society B 285:20181314.

Miller, E. C., C. M. Martinez, S. T. Friedmand, P. C. Wainwright, S. A. Price, and L. Tornabene. 2022. Alternating regimes of shallow and deep-sea diversification explain a species-richness paradox in marine fishes. Proceedings of the National Academy of Sciences of the USA 119:e21235441.

Miller, E. C., S. L. Mesnick, and J. J. Wiens. 2021. Sexual dichromatism is decoupled from diversification over deep time in fishes. American Naturalist 198:232–252.

Miller, E. C., and C. Román-Palacios. 2021. Evolutionary time best explains the latitudinal diversity gradient of living freshwater fish diversity. Global Ecology and Biogeography 30:749–763.

Mirarab, S., and T. Warnow. 2015. ASTRAL-II: coalescent-based species tree estimation with many hundreds of taxa and thousands of genes. Bioinformatics 31:i44–i52.

Mittelbach, G. G., D. W. Schemske, H. V. Cornell, A. P. Allen, J. M. Brown, M. B. Bush, S. P. Harrison, et al. 2007. Evolution and the latitudinal diversity gradient: speciation, extinction and biogeography. Ecology Letters 10:315–331.

Mouillot, D., S. Villéger, V. Parravicini, M. Kulbicki, J. E. Arias-González, M. Bender, P. Chabanet, et al. 2014. Functional over-redundancy and high functional vulnerability in global fish faunas on tropical reefs. Proceedings of the National Academy of Sciences of the USA 111:13757–13762.

Nash, C. M., L. L. Lungstrom, L. C. Hughes, and M. W. Westneat. 2022. Phylogenomics and body shape morphometrics reveal recent diversification in the goatfishes (Syngnatharia: Mullidae). Molecular Phylogenetics and Evolution 177:107616.

Neutens, C., D. Adriaens, J. Christiaens, B. De Kegel, M. Dierick, R. Boistel, and L. Van Hoorebeke. 2014. Grasping convergent evolution in syngnathids: a unique tale of tails. Journal of Anatomy 224:710–723.

Pohlert, T. 2021. Package PMCMRplus. R Package version 4.1. https://cran.r-project.org/web/packages/PMCMRplus/index.html.

Price, S. A., T. Claverie, T. J. Near, and P. C. Wainwright. 2015. Phylogenetic insights into the history and diversification of fishes on reefs. Coral Reefs 34:997–1009.

Pyron, R. A., and J. J. Wiens. 2013. Large-scale phylogenetic analyses reveal the causes of high tropical amphibian diversity. Proceedings of the Royal Society B 280:20131622.

Rabosky, D. L. 2010. Extinction rates should not be estimated from molecular phylogenies. Evolution 64:1816–1824.

Rabosky, D. L., J. Chang, P. O. Title, P. F. Cowman, L. Sallan, M. Friedman, K. Kaschner, et al. 2018. An inverse latitudinal gradient in speciation rate for marine fishes. Nature 559:392–395.

Rabosky, D. L., M. Grundler, C. Anderson, P. Title, J. J. Shi, J. W. Brown, H. Huang, and J. G. Larson. 2014. BAMMtools: an R package for the analysis of evolutionary dynamics on phylogenetic trees. Methods in Ecology and Evolution 5:701–707.

Ree, R. H., and I. Sanmartín. 2018. Conceptual and statistical problems with the DEC+J model of founder-event speciation and its comparison with DEC via model selection. Journal of Biogeography 45:741–749.

Renema, W., D. R. Bellwood, J. C. Braga, K. Bromfield, R. Hall, K. G. Johnson, P. Lunt, et al. 2008. Hopping hotspots: global shifts in marine biodiversity. Science 321:654–657.

Revell, L. J. 2012. phytools: an R package for phylogenetic comparative biology (and other things). Methods in Ecology and Evolution 3:217–223.

Ricklefs, R. E. 1987. Community diversity: relative roles of local and regional processes. Science 235:167–171.

———. 2012. Species richness and morphological diversity of passerine birds. Proceedings of the National Academy of Sciences of the USA 109:14482–14487.

Rincon-Sandoval, M., E. Duarte-Ribeiro, A. M. Davis, A. Santaquiteria, L. C. Hughes, C. C. Baldwin, L. Soto-Torres, et al. 2020. Evolutionary determinism and convergence associated with water-column transitions in marine fishes. Proceedings of the National Academy of Sciences of the USA 117:33396–33403.

Rohde, K. 1992. Latitudinal gradients in species diversity: the search for the primary cause. Oikos 65:514–527.

Rolland, J., F. L. Condamine, F. Jiguet, and H. Morlon. 2014. Faster speciation and reduced extinction in the tropics contribute to the mammalian latitudinal diversity gradient. PLoS Biology 12:e1001775.

Sallan, L. C., and M. Friedman. 2012. Heads or tails: staged diversification in vertebrate evolutionary radiations. Proceedings of the Royal Society B 279:2025–2032.

Sanciangco, J. C., K. E. Carpenter, P. J. Etnoyer, and F. Moretzsohn. 2013. Habitat availability and heterogeneity and the Indo-Pacific warm pool as predictors of marine species richness in the tropical Indo-Pacific. PLoS ONE 8:e56245.

Santaquiteria, A., E. C. Miller, U. Rosas-Puchuri, C. del R. Pedraza-Marrón, E. M. Troyer, M. W. Westneat, G. Carnevale, D. Arcila, and R. Betancur. 2024. Data from: Colonization dynamics explain the decoupling of species richness and morphological disparity in syngnatharian fishes across oceans. American Naturalist, Dryad Digital Repository, https://doi.org/10.5061/dryad.zkh1893gd.

Santaquiteria, A., A. C. Siqueira, E. Duarte-Ribeiro, G. Carnevale, W. T. White, J. J. Pogonoski, C. C. Baldwin, G. Orti, D. Arcila, and R. Betancur. 2021. Phylogenomics and historical biogeography of seahorses, dragonets, goatfishes, and allies (Teleostei: Syngnatharia): assessing factors driving uncertainty in biogeographic inferences. Systematic Biology 70:1145–1162.

Santodomingo, N., C. C. Wallace, and K. G. Johnson. 2015. Fossils reveal a high diversity of the staghorn coral genera *Acropora* and *Isopora* (Scleractinia: Acroporidae) in the Neogene of Indonesia. Zoological Journal of the Linnean Society 175:677–763.

Schluter, D. 2015. Speciation, ecological opportunity, and latitude (American Society of Naturalists address). American Naturalist 187:1–18.

Schwartz, R. S., and R. L. Mueller. 2010. Branch length estimation and divergence dating: estimates of error in Bayesian and maximum likelihood frameworks. BMC Evolutionary Biology 10:5.

Siqueira, A. C., D. R. Bellwood, and P. F. Cowman. 2019. The evolution of traits and functions in herbivorous coral reef fishes through space and time. Proceedings of the Royal Society B 286:20182672.

Siqueira, A. C., R. A. Morais, D. R. Bellwood, and P. F. Cowman. 2020. Trophic innovations fuel reef fish diversification. Nature Communications 11:1–11.

———. 2021. Planktivores as trophic drivers of global coral reef fish diversity patterns. Proceedings of the National Academy of Sciences of the USA 118:e2019404118.

Siqueira, A. C., L. G. R. Oliveira-Santos, P. F. Cowman, and S. R. Floeter. 2016. Evolutionary processes underlying latitudinal differences in reef fish biodiversity. Global Ecology and Biogeography 25:1466–1476.

Smith, S. A., and B. C. O'Meara. 2012. TreePL: divergence time estimation using penalized likelihood for large phylogenies. Bioinformatics 28:2689–2690.

Spalding, M. D., H. E. Fox, G. R. Allen, N. Davidson, Z. A. Ferdaña, M. Finlayson, B. S. Halpern, et al. 2007. Marine ecoregions of the world: a bioregionalization of coastal and shelf areas. BioScience 57:573–583.

Stamatakis, A. 2014. RAxML version 8: a tool for phylogenetic analysis and post-analysis of large phylogenies. Bioinformatics 30:1312–1313.

Steinthorsdottir, M., H. K. Coxall, A. M. de Boer, M. Huber, N. Barbolini, C. D. Bradshaw, N. J. Burls, et al. 2021. The Miocene: the future of the past. Paleoceanography and Paleoclimatology 36:e2020PA004037.

Stephens, P. R., and J. J. Wiens. 2003. Explaining species richness from continents to communities: the time-for-speciation effect in emydid turtles. American Naturalist 161:112–128.

Stiller, J., G. Short, H. Hamilton, N. Saarman, S. Longo, P. Wainwright, G. W. Rouse, and W. B. Simison. 2022. Phylogenomic analysis of Syngnathidae reveals novel relationships, origins of endemic diversity and variable diversification rates. BMC Biology 20:1–21.

Tamura, K., F. U. Battistuzzi, P. Billing-Ross, O. Murillo, A. Filipski, and S. Kumar. 2012. Estimating divergence times in large molecular phylogenies. Proceedings of the National Academy of Sciences of the USA 109:19333–19338.

Title, P. O., and D. L. Rabosky. 2019. Tip rates, phylogenies and diversification: what are we estimating, and how good are the estimates? Methods in Ecology and Evolution 10:821–834.

Tittensor, D. P., C. Mora, W. Jetz, H. K. Lotze, D. Ricard, E. Vanden Berghe, and B. Worm. 2010. Global patterns and predictors of marine biodiversity across taxa. Nature 466:1098–1101.

Uyeda, J. C., D. S. Caetano, and M. W. Pennell. 2015. Comparative analysis of principal components can be misleading. Systematic Biology 64:677–689.

Vasconcelos, T. N. C., S. Alcantara, C. O. Andrino, F. Forest, M. Reginato, M. F. Simon, and J. R. Pirani. 2020. Fast diversification through a mosaic of evolutionary histories characterizes the endemic flora of ancient Neotropical mountains. Proceedings of the Royal Society B 287:20192933.

Wainwright, P. C., and S. J. Longo. 2017. Functional innovations and the conquest of the oceans by acanthomorph fishes. Current Biology 27:R550–R557.

Wainwright, P. C., W. L. Smith, S. A. Price, K. L. Tang, J. S. Sparks, L. A. Ferry, K. L. Kuhn, R. I. Eytan, and T. J. Near. 2012. The evolution of pharyngognathy: a phylogenetic and functional appraisal of the pharyngeal jaw key innovation in labroid fishes and beyond. Systematic Biology 61:1001–1027.

Wallace, C. C., and B. R. Rosen. 2006. Diverse staghorn corals (Acropora) in high-latitude Eocene assemblages: implications for the evolution of modern diversity patterns of reef corals. Proceedings of the Royal Society B 273:975–982.

Williams, S. T., and T. F. Duda. 2008. Did tectonic activity stimulate Oligo-Miocene speciation in the Indo-West Pacific? Evolution 62:1618–1634.

Woodland, D. J. 1983. Zoogeography of the Siganidae (Pisces): an interpretation of distribution and richness patterns (Indo-Pacific). Bulletin of Marine Science 33:713–717.

Xing, Y., and R. H. Ree. 2017. Uplift-driven diversification in the Hengduan Mountains, a temperate biodiversity hotspot. Proceedings of the National Academy of Sciences of the USA 114: E3444–E3451.

References Cited Only in the Online Enhancements

Adams, C. G., A. W. Gentry, and P. J. Whybrow. 1983. Dating the terminal Tethyan event. Utrecht Micropaleontological Bulletins 30:273–298.

Adams, D. C., and M. L. Collyer. 2018. Phylogenetic ANOVA: group-clade aggregation, biological challenges, and a refined permutation procedure. Evolution 72:1204–1215.

Alfaro, M. E., B. C. Faircloth, R. C. Harrington, L. Sorenson, M. Friedman, C. E. Thacker, C. H. Oliveros, D. Černý, and T. J. Near. 2018. Explosive diversification of marine fishes at the Cretaceous-Palaeogene boundary. Nature Ecology and Evolution 2:688–696.

Bachmayer, F. 1980. Eine fossile Schlangennadel (Syngnathidae) aus dem Leithakalk (Badenien) von St. Margarethen, Burgenland (Österreich). Annalen des Naturhistorischen Museums in Wien 83:29–33.

Bannikov, A. F., and G. Carnevale. 2012. A long-bodied centriscoid fish from the basal Eocene of Kabardino-Balkaria, northern Caucasus, Russia. Naturwissenschaften 99:379–389.

Beaulieu, J. M., and B. C. O'Meara. 2016. Detecting hidden diversification shifts in models of trait-dependent speciation and extinction. Systematic Biology 65:583–601.

Beluzhenko, E. V. 2002. Stratigrafiya sredne-verkhnemiotsenovykh i pliotsenovykh otlozheniy mezhdurech'ya Psekups–Belaya (Severo-Za-padnyj Kavkaz). 1. Sredniy miotsen. Bulletin of Moscow Society of Naturalists. Geological Series 77:47–59. [In Russian.]

Betancur-R., R., E. O. Wiley, G. Arratia, A. Acero, N. Bailly, M. Miya, G. Lecointre, and G. Ortí. 2017. Phylogenetic classification of bony fishes. BMC Evolutionary Biology 17:162.

Blot, J. 1980. The ichthyofauna of the deposits of Monte Bolca (Province de Vérone, Italie). Catalogue systématique présentat l'état actuel des recherches concernant cette faune. Bulletin du Muséum National d'Histoire Naturelle C 2:339–396.

Bouckaert, R. R. 2010. DensiTree: making sense of sets of phylogenetic trees. Bioinformatics 26:1372–1373.

Caldwell, M. K. 1962. Development and distribution of larval and juvenile fishes of the family Mullidae of the western North Atlantic. Fishery Bulletin 62:403–457.

Calzoni, P., J. Amalfitano, L. Giusberti, G. Marramà, and G. Carnevale. 2023. Eocene Rhamphosidae (Teleostei: Syngnathiformes) from the Bolca Lagerstätte, Italy. Rivista Italiana Di Paleontologia E Stratigrafia 129:573–607.

Carnevale, G., and A. F. Bannikov. 2019. A dragonet (Teleostei, callionymoidei) from the Eocene of Monte Bolca, Italy. Bollettino della Societa Paleontologica Italiana 58:295–307.

Carnevale, G., A. F. Bannikov, W. Landini, and C. Sorbini. 2006. Volhynian (early Sarmatian sensu lato) fishes from Tsurevsky, North Caucasus, Russia. Journal of Paleontology 80:684–699.

Claverie, T., and P. C. Wainwright. 2014. A morphospace for reef fishes: elongation is the dominant axis of body shape evolution. PLoS ONE 9:e112732.

Coates, A. G., and J. A. Obando. 1996. The geologic evolution of the Central American isthmus. Pages 21–56 *in* J. B. C. Jackson, A. F. Budd, and A. G. Coates, eds. Evolution and environment in tropical America. University of Chicago Press, Chicago.

Felsenstein, J. 1985. Phylogenies and the comparative method. American Naturalist 125:1–15.

Friedman, M., K. L. Feilich, H. T. Beckett, M. E. Alfaro, B. C. Faircloth, D. Černý, M. Miya, T. J. Near, and R. C. Harrington. 2019. A phylogenomic framework for pelagiarian fishes (Acanthomorpha: Percomorpha) highlights mosaic radiation in the open ocean. Proceedings of the Royal Society B 286:20191502.

Gavrilov, Y., E. Shcherbinina, and H. Oberhänsli. 2003. Paleocene-Eocene boundary events in the northeastern Peri-Tethys. Geological Society of America Special Papers 369:147–168.

GBIF (Global Biodiversity Information Facility). 2022. Global Biodiversity Information Facility. https://www.gbif.org/.

Goldberg, E. E., L. T. Lancaster, and R. H. Ree. 2011. Phylogenetic inference of reciprocal effects between geographic range evolution and diversification. Systematic Biology 60:451–465.

Harmon, L. J., J. T. Weir, C. D. Brock, R. E. Glor, and W. Challenger. 2008. GEIGER: investigating evolutionary radiations. Bioinformatics 24:129–131.

Harrington, R. C., B. C. Faircloth, R. I. Eytan, W. L. Smith, T. J. Near, M. E. Alfaro, and M. Friedman. 2016. Phylogenomic analysis of carangimorph fishes reveals flatfish asymmetry arose in a blink of the evolutionary eye. BMC Evolutionary Biology 16:1–14.

Hedman, M. M. 2010. Constraints on clade ages from fossil outgroups. Paleobiology 36:16–31.

IUCN. 2021. The IUCN Red List of Threatened Species. https://www.iucnredlist.org/.

Jombart, T., M. Kendall, J. Almagro-Garcia, and C. Colijn. 2017. treespace: statistical exploration of landscapes of phylogenetic trees. Molecular Ecology Resources 17:1385–1392.

Jordan, D. S., and B. W. Evermann. 1898. The fishes of north and middle America: a descriptive catalogue of the species of fish-like vertebrates found in the waters of North America, north of the Isthmus of Panama. II. Bulletin of the United States National Museum 47: 1241–2183.

Landis, M. J., N. J. Matzke, B. R. Moore, and J. P. Huelsenbeck. 2013. Bayesian analysis of biogeography when the number of areas is large. Systematic Biology 62:789–804.

Lloyd, G. T., D. W. Bapst, M. Friedman, and K. E. Davis. 2016. Probabilistic divergence time estimation without branch lengths: dating the origins of dinosaurs, avian flight and crown birds. Biology Letters 12:20160609.

Matzke, N. J. 2014. Model selection in historical biogeography reveals that founder-event speciation is a crucial process in island clades. Systematic Biology 63:951–970.

Mello, B., Q. Tao, J. Barba-Montoya, and S. Kumar. 2021. Molecular dating for phylogenies containing a mix of populations and species by using Bayesian and RelTime approaches. Molecular Ecology Resources 21:122–136.

Montes, C., A. Cardona, C. Jaramillo, A. Pardo, C. Silva, V. Valencia, C. Ayala, et al. 2015. Middle Miocene closure of the Central American seaway. Science 348:226–229.

Nielsen, E. 1960. A new Eocene teleost from Denmark. Meddelelser fra Dansk Geologisk Forening 14:247–252.

OBIS (Ocean Biogeographic Information System). 2021. Data from the Ocean Biogeographic Information System. Intergovernmental Oceanographic Commission of UNESCO, Paris. https://obis.org/.

O'Dea, A., H. A. Lessios, A. G. Coates, R. I. Eytan, S. A. Restrepo-Moreno, A. L. Cione, et al. 2016. Formation of the Isthmus of Panama. Science Advances 2:1–12.

Papazzoni, C. A., G. Carnevale, E. Fornaciari, L. Giusberti, and E. Trevisani. 2014. The Pesciara-Monte Postale Fossil-Lagerstätte. 1. Biostratigraphy, sedimentology and depositional model. Pages 29–36 *in* C. A. Papazzoni, L. Giusberti, G. Carnevale, G. Roghi, D. Bassi, and R. Zorzin, eds. The Bolca Fossil-Lagerstätten: a window into the Eocene World. Rendiconti della Società Paleontologica Italiana 4. Società Paleontologica Italiana, Modena.

Parham, J. F., P. C. J. Donoghue, C. J. Bell, T. D. Calway, J. J. Head, P. A. Holroyd, J. G. Inoue, et al. 2012. Best practices for justifying fossil calibrations. Systematic Biology 61:346–359.

Parin, N., and N. Micklich. 1996. Fossil gasterosteiformes from the lower Oligocene of Frauenweiler (Baden-Württemberg, Germany). I. New information on the morphology and systematics of the genus *Aeoliscus* Jordan & Starks 1902. Paläontologische Zeitschrift 70:521–545.

Peterson, R. D., J. P. Sullivan, C. D. Hopkins, A. Santaquiteria, C. B. Dillman, S. Pirro, R. Betancur-R., D. Arcila, L. C. Hughes, and G. Ortí. 2022. Phylogenomics of bony-tongue fishes (Osteoglossomorpha) shed light on the craniofacial evolution and biogeography of the weakly electric clade (Mormyridae). Systematic Biology 71:1032–1044.

Pietsch, T. 1978. Evolutionary relationships of the sea moths (Teleostei: Pegasidae) with a classification of gasterosteiform families. Copeia 1978:517–529.

Plummer, M., N. Best, K. Cowles, and K. Vines. 2006. CODA: convergence diagnosis and output analysis for MCMC. R News 6:7–11.

Popov, Y. A. 2017. First record of the pipefish *Nerophis zapfei* Bachmayer (Syngnathidae, Gasterosteiformes) from the Middle Miocene of northern Moldova. Paleontological Journal 51:533–541.

Price, M. N., P. S. Dehal, and A. P. Arkin. 2010. FastTree 2: approximately maximum-likelihood trees for large alignments. PLoS ONE 5:e9490.

QGIS Development Team. 2009. QGIS Geographic Information System. Open Source Geospatial Foundation.

Rabosky, D. L. 2014. Automatic detection of key innovations, rate shifts, and diversity-dependence on phylogenetic trees. PLoS ONE 9:e89543.

Rambaut, A., A. J. Drummond, D. Xie, G. Baele, and M. A. Suchard. 2018. Posterior summarization in Bayesian phylogenetics using Tracer 1.7. Systematic Biology 67:901–904.

Ranwez, V., E. J. P. Douzery, C. Cambon, N. Chantret, and F. Delsuc. 2018. MACSE v2: toolkit for the alignment of coding sequences accounting for frameshifts and stop codons. Molecular Biology and Evolution 35:2582–2584.

Ree, R. H., and S. A. Smith. 2008. Maximum likelihood inference of geographic range evolution by dispersal, local extinction, and cladogenesis. Systematic Biology 57:4–14.

Rögl, F. 1999. Palaeogeographic considerations for Mediterranean and Paratethys seaways. Annalen des Naturhistorischen Museums in Wien 99A:279–310.

Ronquist, F. 1997. Dispersal-vicariance analysis: a new approach to the quantification of historical biogeography. Systematic Biology 46:195–203.

Schmid, H. P., M. Harzhauser, and A. Kroh. 2001. Hypoxic events on a Middle Miocene carbonate platform of the central Paratethys (Austria, Badenian, 14 Ma), with contribution by Coric S., Rögl F. & Schultz O. Annalen des Naturhistorischen Museums in Wien 95A:127–177.

Schmitz, B., B. Peucker-Ehrenbrink, C. Heilmann-Clausen, G. Åberg, F. Asaro, and C. T. A. Lee. 2004. Basaltic explosive volcanism, but no comet impact, at the Paleocene-Eocene boundary: high-resolution chemical and isotopic records from Egypt, Spain and Denmark. Earth and Planetary Science Letters 225:1–17.

Stecher, G., K. Tamura, and S. Kumar. 2020. Molecular evolutionary genetics analysis (MEGA) for macOS. Molecular Biology and Evolution 37:1237–1239.

Steininger, F., and F. Rögl. 1979. The paratethys history: a contribution towards the Neogene geodynamics of the Alpine orogene. Annales Geologiques des Pays Helleniques 3:1153–1165.

Storey, M., R. A. Duncan, and C. C. Swisher. 2007. Paleocene-Eocene thermal maximum and the opening of the northeast Atlantic. Science 316:587–589.

Tamura, K., Q. Tao, and S. Kumar. 2018. Theoretical foundation of the RelTime method for estimating divergence times from variable evolutionary rates. Molecular Biology and Evolution 35: 1770–1782.

Volta, G. 1796. Ittiolitologia Veronese del Museo Bozziano ora annesso a quello del Conte Giovambattista Gazola e di altri gabinetti di fossili veronesi. Stamperia Giularia, Verona.

Wickham, H. 2008. ggplot2: elegant graphics for data analysis. Springer, Cham.

Yang, C., Y. Zheng, S. Tan, G. Meng, W. Rao, C. Yang, D. G. Bourne, et al. 2020. Efficient COI barcoding using high throughput single-end 400 bp sequencing. BMC Genomics 21:1–10.

Yang, Z. 2007. PAML 4: phylogenetic analysis by maximum likelihood. Molecular Biology and Evolution 8:1586–1591.

Zhang, C., M. Rabiee, E. Sayyari, and S. Mirarab. 2018. ASTRAL-III: polynomial time species tree reconstruction from partially resolved gene trees. BMC Bioinformatics 19:153.

Associate Editor: Marjorie G. Weber
Editor: Volker H. W. Rudolf

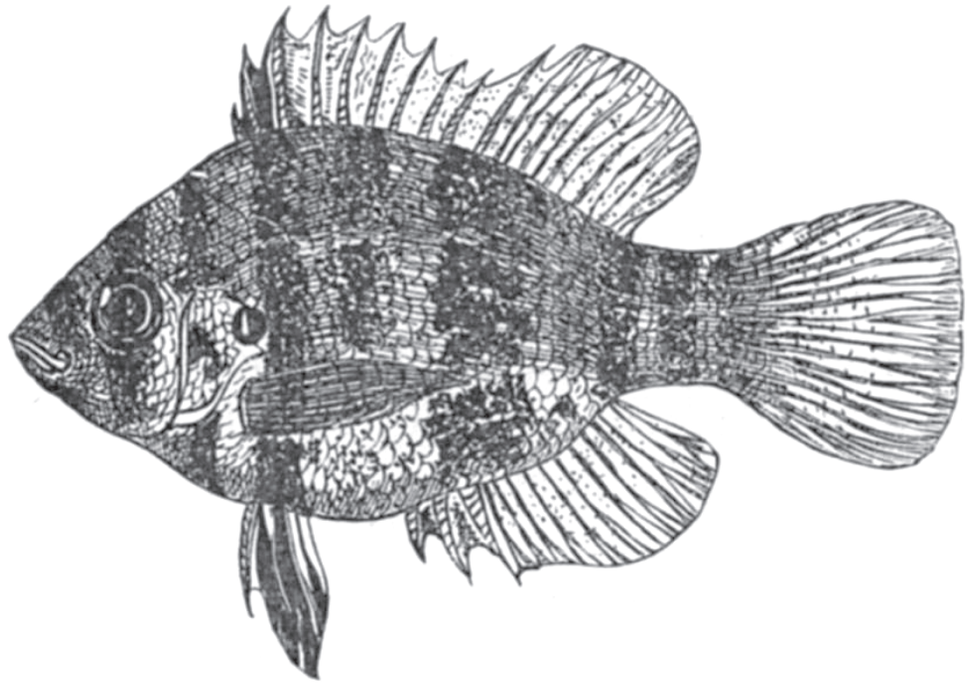

"Although so small, it is a plucky fish, and promptly resents any interference. Being a feeble swimmer, it depends, for defense, upon the sharp spines of its dorsal fin, and it seems to know that when these are erected it is quite free from molestation. Especially angry does it become when a great lubberly catfish chances to wander by and pokes his slimy nose into its haunts. At once the 'bandy' is up in arms, and darts at the intruder with great violence." Figured: "Banded Sunfish (*Mesogonistius chætodon*)." From "On the Habits of Certain Sunfish" by C. C. Abbott (*The American Naturalist*, 1883, 17:1254–1257).